

Mixed Higgsino Dark Matter from a Large $SU(2)$ Gaugino Mass

Howard Baer^a, Azar Mustafayev^b, Heaya Summy^a and Xerxes Tata^c

^a*Department of Physics, Florida State University Tallahassee, FL 32306, USA*

^b*Dept. of Physics and Astronomy, University of Kansas, Lawrence, KS 66045, USA*

^c*Department of Physics and Astronomy, University of Hawaii, Honolulu, HI 96822, USA*

E-mail: baer@hep.fsu.edu, amustaf@ku.edu,
heaya@hep.fsu.edu, tata@phys.hawaii.edu

ABSTRACT: We observe that in SUSY models with non-universal GUT scale gaugino mass parameters, raising the GUT scale $SU(2)$ gaugino mass $|M_2|$ from its unified value results in a smaller value of $-m_{H_u}^2$ at the weak scale. By the electroweak symmetry breaking conditions, this implies a reduced value of μ^2 *vis à vis* models with gaugino mass unification. The lightest neutralino can then be mixed Higgsino dark matter with a relic density in agreement with the measured abundance of cold dark matter (DM). We explore the phenomenology of this high $|M_2|$ DM model. The spectrum is characterized by a very large wino mass and a concomitantly large splitting between left- and right- sfermion masses. In addition, the lighter chargino and three light neutralinos are relatively light with substantial higgsino components. The higgsino content of the LSP implies large rates for direct detection of neutralino dark matter, and enhanced rates for its indirect detection relative to mSUGRA. We find that experiments at the LHC should be able to discover SUSY over the portion of parameter space where $m_{\tilde{g}} \lesssim 2350 - 2750$ GeV, depending on the squark mass, while a 1 TeV electron-positron collider has a reach comparable to that of the LHC. The dilepton mass spectrum in multi-jet + $\ell^+ \ell^- + E_T^{\text{miss}}$ events at the LHC will likely show more than one mass edge, while its shape should provide indirect evidence for the large higgsino content of the decaying neutralinos.

KEYWORDS: Supersymmetry Phenomenology, Supersymmetric Standard Model, Dark Matter.

1. Introduction and framework

There is overwhelming evidence showing that most of the matter in the Universe is not baryonic, but composed of a new massive stable (or at least very long-lived), weakly (or super-weakly) interacting particle not contained in the Standard Model (SM) of particle physics. Moreover, the mass density of this cold “dark matter” (DM) has been precisely measured: combining the results from the WMAP Collaboration with those from the Sloan Digital Sky Survey gives [1]

$$\Omega_{\text{DM}}h^2 = 0.111_{-0.015}^{+0.011} \quad (2\sigma), \quad (1.1)$$

where $\Omega = \rho/\rho_c$ with ρ_c the closure density of the Universe, and h is the scaled Hubble parameter, $h = 0.73 \pm 0.04$. While the mass density of DM is rather precisely known, the identity of DM remains a mystery. Like visible matter, the DM may well consist of several components, in which case the density in (1.1) yields an *upper limit* on the density of any single component. Supersymmetric (SUSY) models of particle physics with a conserved R -parity include a stable, massive interacting particle, often the lightest neutralino \tilde{Z}_1 . Remarkably, the properties of the neutralino are just right to enable it to serve as *thermally produced* dark matter within the standard Big Bang cosmology if the SUSY mass scale is ~ 100 GeV [2, 3].¹

A potential sticking point in the discussion of SUSY DM is that the non-observation of direct or indirect effects of SUSY are beginning to push M_{SUSY} beyond 100 GeV. As a result, the neutralino annihilation cross-section which is $\propto 1/M_{\text{SUSY}}^2$ is correspondingly reduced, and the calculated neutralino relic abundance is typically considerably larger [5] than the value in Eq. (1.1). For instance, in the mSUGRA model [6], almost all of parameter space is excluded by the precisely measured abundance, and only a few distinct regions where neutralino annihilation is enhanced survive: the nearly excluded bulk region with low masses already mentioned above [7], the stau[8] or stop[9] co-annihilation regions, the hyperbolic branch/focus point (HB/FP) region at large m_0 [10], where the \tilde{Z}_1 becomes mixed higgsino dark matter (with enhanced annihilation to W and Z particles via its higgsino component), or the A or h resonance annihilation (Higgs funnel) region[11, 12]. Within the mSUGRA framework, each of these regions leads to characteristic patterns in collider signals at the soon-to-be-operational CERN Large Hadron Collider (LHC), and also to differences in signals in direct and indirect DM search experiments under way.

We recognize, however, that these conclusions about the expected patterns are specific to the mSUGRA model, and can be obviated in simple extensions of this framework where new mechanisms may arise to match the predicted neutralino abundance to the measured CDM density. In previous works, in the scalar sector, non-universal soft masses for the different generations[13], or for the Higgs scalars have been considered[14]. In the gaugino

¹It is possible to invoke models where the DM results from late decays of heavy particles and so is not in thermal equilibrium, or to invoke non-standard Big Bang cosmologies [4] to obtain the observed value of the DM density. It is, nevertheless, appealing if we can account for the relic density data with minimal assumptions: *i.e.* via thermally produced relics within the standard Big Bang model.

sector, by abandoning gaugino mass universality at the GUT scale, a variety of new mechanisms emerge.² As shown in Ref. [16, 17], allowing the weak scale gaugino masses $M_1 \sim M_2$ gives rise to mixed wino dark matter (MWDM), wherein $\tilde{Z}_1\tilde{Z}_1 \rightarrow W^+W^-$ is enhanced in the early Universe. Alternatively, if GUT scale parameters are such that $M_1 \sim -M_2$ at the weak scale, then there is little bino-wino mixing, but neutralino annihilation is enhanced in the early Universe because of bino-wino co-annihilation[18] (BWCA). Finally, if the $SU(3)$ gaugino mass $M_3 \ll M_1 \sim M_2$ at the GUT scale, then the Higgs mass parameter $m_{H_u}^2$ is driven to less negative values at the weak scale, so that $\mu^2 \sim -m_{H_u}^2$ is also small, resulting in mixed higgsino dark matter (MHDM) [19, 20]. These models, wherein the composition of the neutralino is adjusted to get the correct dark matter abundance, are collectively dubbed “well-tempered neutralino” models[21], with typical neutralino-nucleon scattering cross sections $\sigma(\tilde{Z}_1p) \sim 10^{-8}$ pb [22], which is within an order of magnitude of the sensitivity of current experiments. It is instructive to note that each of these alternatives can arise in the top-down approach of string-inspired mixed moduli-anomaly mediated SUSY breaking (mirage unification) models[23]. It should also be noted that the low M_3 framework with its concomitantly light squarks offers a novel possibility for getting agreement with (1.1) if the rate for $\tilde{Z}_1\tilde{Z}_1 \rightarrow t\bar{t}$ is unsuppressed because \tilde{t}_1 is relatively light [24]; the phenomenology of such a scenario has recently been detailed in Ref. [25].

In this paper, we present a novel possibility, again based on non-universal gaugino mass parameters at the GUT scale, for obtaining agreement with (1.1) via MHDM. We assume that the MSSM as the correct effective field theory valid between energy scales $Q \sim M_{\text{weak}}$ and $Q = M_{GUT} \sim 2 \times 10^{16}$ GeV (for text book accounts, see Ref. [26, 27]). We adopt the usual universality of scalar mass parameters and trilinear scalar couplings but take GUT scale boundary conditions in the gaugino sector of the form $M_2 \gg M_1 \sim M_3$. We then inspect the evolution of the soft term $m_{H_u}^2$ whose 1-loop RGE is given by

$$\frac{dm_{H_u}^2}{dt} = \frac{2}{16\pi^2} \left(-\frac{3}{5}g_1^2M_1^2 - 3g_2^2M_2^2 + \frac{3}{10}g_1^2S + 3f_t^2X_t \right), \quad (1.2)$$

where $t = \log Q^2$, f_t is the top quark Yukawa coupling, $X_t = m_{Q_3}^2 + m_{\tilde{t}_R}^2 + m_{H_u}^2 + A_t^2$ and $S = m_{H_u}^2 - m_{H_d}^2 + \text{Tr}(\mathbf{m}_Q^2 - \mathbf{m}_L^2 - 2\mathbf{m}_U^2 + \mathbf{m}_D^2 + \mathbf{m}_E^2)$. Usually, the $f_t^2X_t$ term overcomes the upward push from the gauge-gaugino terms (proportional to the gaugino mass parameters) and drives $m_{H_u}^2$ to lower values as Q is reduced, and ultimately to negative values, the celebrated radiative electroweak symmetry breaking (REWSB) mechanism[28]. In the case where M_2 is very large at the GUT scale, the gaugino terms initially win resulting in an *upwards* push at the start of the $m_{H_u}^2$ evolution. The large M_2 also increases the various left- scalar soft masses to initially large values, thus enhancing the magnitude of X_t which results in an increased *downward* push of the $f_t^2X_t$ term. The resulting value of $m_{H_u}^2$ (weak) depends on the value of $M_2(\text{GUT})$; by adjusting the latter we can arrange things so that by the time the weak scale is reached, the (incomplete) cancellation between the upwards and downwards push results in a negative value of $m_{H_u}^2$ that is significantly smaller in

²Non-universal gaugino masses can be accommodated in SUSY GUT if the auxiliary field that breaks supersymmetry also breaks the GUT symmetry [15].

magnitude than in models where GUT scale gaugino mass parameters have a common value. The weak scale value of μ^2 (at tree-level) is then obtained from the weak scale parameters of the Higgs sector via the EWSB relation,

$$\mu^2 = \frac{m_{H_d}^2 - m_{H_u}^2 \tan^2 \beta}{(\tan^2 \beta - 1)} - \frac{M_Z^2}{2}. \quad (1.3)$$

We see that if $|m_{H_u}^2| \gg M_Z^2$ and for moderate to large values of $\tan \beta$, $\mu^2 \sim -m_{H_u}^2$. Thus, the small $|m_{H_u}^2|$ value results in a smaller $|\mu|$ parameter, and a correspondingly larger higgsino component of the lightest neutralino \tilde{Z}_1 . As discussed above, MHDM can easily be compatible with the observed relic density because the neutralino annihilation into WW , ZZ and Zh pairs is enhanced on account of the higgsino content of \tilde{Z}_1 . Since the large value of the wino mass underlies the root of this scenario, we will call it the high M_2 dark matter (HM2DM) model.

The situation is illustrated in Fig. 1. The model is specified by the mSUGRA parameter set augmented by one additional parameter, M_2 :

$$m_0, m_{1/2}, M_2, A_0, \tan \beta \text{ and } \text{sign}(\mu), \quad (1.4)$$

where $M_1 = M_3 \equiv m_{1/2}$, but M_2 is allowed to be free (with either sign). We take $m_t = 171.4$ GeV, in accord with recent mass determinations[29]. We illustrate in Fig. 1a) the evolution of $\text{sign}(m_{H_u}^2)\sqrt{|m_{H_u}^2|}$ and $\text{sign}(m_{H_d}^2)\sqrt{|m_{H_d}^2|}$ as a function of scale Q in the mSUGRA model (solid) for $m_0 = 300$ GeV, $m_{1/2} = 300$ GeV, $A_0 = 0$, $\tan \beta = 10$, $\mu > 0$.

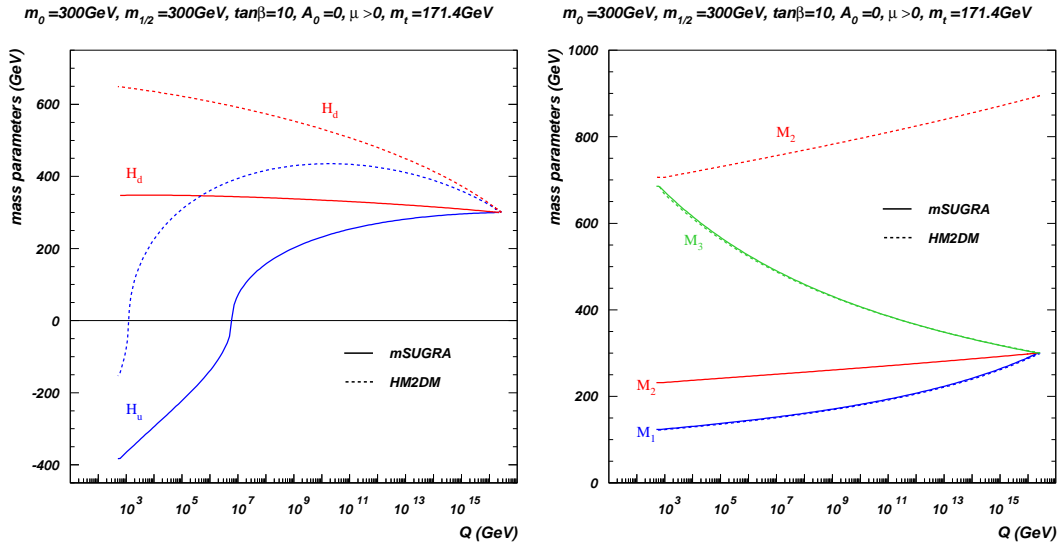


Figure 1: Evolution of a) the soft SUSY breaking Higgs mass parameters $\text{sign}(m_{H_u}^2)\sqrt{|m_{H_u}^2|}$ and $\text{sign}(m_{H_d}^2)\sqrt{|m_{H_d}^2|}$, and b) the gaugino mass parameters, as a function of the energy scale Q in the mSUGRA model (solid) for $m_0 = 300$ GeV, $m_{1/2} = 300$ GeV, $A_0 = 0$, $\tan \beta = 10$, $\mu > 0$ and $m_t = 171.4$ GeV, and for the HM2DM model (dashes). The model parameters adopted for HM2DM are the same as in the mSUGRA case except that $M_2 = 3m_{1/2}$ at $Q = M_{GUT}$.

The same running mass parameters are shown for HM2DM for the same parameters as in the mSUGRA case except that we now take $M_2 = 3m_{1/2}$ at $Q = M_{\text{GUT}}$ (dashes). In the mSUGRA case, $m_{H_u}^2$ evolves from a positive GUT scale value to a large negative value at $Q = M_{\text{weak}}$, resulting in a large $|\mu|$ parameter. In the case of HM2DM, however, the large value of M_2 initially causes $m_{H_u}^2$ to evolve *upwards*, but ultimately, the $f_t^2 X_t$ term wins out and $m_{H_u}^2$ evolves to a not-as-large negative value and electroweak symmetry is broken. The smaller value of $-m_{H_u}^2$ at the weak scale leads, of course, to a correspondingly smaller value of $|\mu|$ compared to the mSUGRA case. In Fig. 1b), we show the evolution of gaugino masses in mSUGRA and in the HM2DM case. For mSUGRA, we are left with the gaugino masses at the weak scale in the well-known ratio of $M_1 : M_2 : M_3 \sim 1 : 2 : 7$ which implies (when $|\mu|$ is large) that $m_{\tilde{Z}_1} : m_{\tilde{W}_1} : m_{\tilde{g}} \sim 1 : 2 : 7$. In contrast, in the HM2DM scenario, we have at the weak scale $M_1 \ll M_3 \sim M_2$, so that we expect in general the $SU(2)$ winos to be similar in mass to gluinos, and hence almost decoupled at the LHC.³

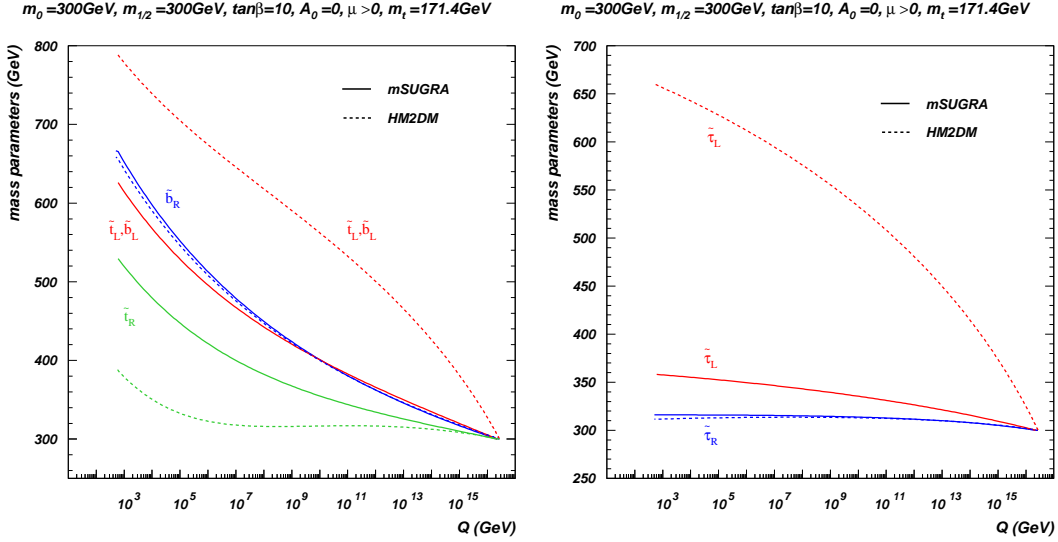


Figure 2: a) Evolution of the soft SUSY breaking squark mass parameters $m_{\tilde{t}_L}$ and $m_{\tilde{t}_R}$ as a function of scale Q in the mSUGRA model (solid) for $m_0 = 300$ GeV, $m_{1/2} = 300$ GeV, $A_0 = 0$, $\tan\beta = 10$, $\mu > 0$ and $m_t = 171.4$ GeV. The same running mass parameters are shown for HM2DM model for the same parameters as in the mSUGRA case except that we take $M_2 = 3m_{1/2}$ at M_{GUT} (dashes). b) Evolution of third generation soft SUSY breaking slepton mass parameters $m_{\tilde{\tau}_L}$ and $m_{\tilde{\tau}_R}$ as a function of scale Q for the same case as in frame a).

The large value of M_2 in the HM2DM model also influences the evolution of matter scalar mass parameters. In Fig. 2a), we show the evolution of third generation squark mass soft parameters versus energy scale for the mSUGRA and the HM2DM models. In the mSUGRA case, we see the hierarchy $m_{\tilde{b}_R} > m_{\tilde{t}_L} > m_{\tilde{t}_R}$ generated by the large top

³The reader may well wonder whether it is possible to obtain MHDM by increasing M_1 instead of M_2 . This does not, however, appear to be possible because the bino mass required for this is so large that, though μ is indeed reduced, the lightest neutralino dominantly becomes a wino-higgsino mixture and annihilates too rapidly to saturate (1.1).

quark Yukawa coupling. However, in the HM2DM case, the large value of M_2 causes left-matter scalars (which have gauge couplings to the heavy winos) to evolve to larger values, so we get large weak scale value of $m_{\tilde{t}_L} (= m_{\tilde{b}_L})$, and also for first and second generation left-sfermions. In addition, the large $m_{\tilde{t}_L}$ enters via the $f_t^2 X_t$ term in the RGE for $m_{\tilde{t}_R}^2$, causing it to reduce at the weak scale. Thus, in HM2DM, we expect large $L - R$ splitting in the squark sector, with $m_{\tilde{t}_L} (= m_{\tilde{b}_L}) > m_{\tilde{b}_R} > m_{\tilde{t}_R}$. As a result, in contrast to the mSUGRA framework, the lighter sbottom quark \tilde{b}_1 is dominantly \tilde{b}_R in the HM2DM scenario.

In Fig. 2*b*), we show the evolution of third generation slepton masses. In the mSUGRA case, there is only a small intra-generation splitting at the weak scale. In the HM2DM scenario, $m_{\tilde{\tau}_R}$ evolves as in mSUGRA, but $m_{\tilde{\tau}_L}$ gains a big enhancement from the large value of M_2 . Thus again, in the slepton sector, we expect large left-right splitting of slepton mass parameters in HM2DM, with left sleptons much heavier than the right sleptons. A similar behaviour is expected for the first two generations of sleptons.

The upshot is that if a large M_2 parameter is the underlying reason for MHD in our Universe, then characteristic sparticle mass spectra and sparticle mixing patterns should emerge as a result. Our goal in this paper is to lay out the phenomenology of this framework. In Sec. 2 we explore the sparticle mass and mixing patterns, and delineate the allowed parameter space in the HM2DM scenario. In Sec. 3, we examine the low energy constraints from $b \rightarrow s\gamma$ and the SUSY contributions to the anomalous magnetic moment of the muon. In Sec. 4, we examine prospects for direct and indirect dark matter detection in the HM2DM framework. In Sec. 5, we examine collider implications of the HM2DM scenario. We end in Sec. 6 with a summary of our results.

2. Parameter space, relic density and mass spectrum

As discussed in the last section, the HM2DM model is completely specified by the parameter set (1.4),

$$m_0, m_{1/2}, M_2, A_0, \tan\beta \text{ and } \text{sign}(\mu),$$

where we assume that $M_1 = M_3 \equiv m_{1/2} \geq 0$ at $Q = M_{GUT}$, and where M_2 can assume either sign. The assumed equality of M_1 and M_3 can be relaxed somewhat and our conclusions suffer little qualitative change so long as $M_2 \gg M_1$. To calculate the sparticle mass spectrum, we use Isajet 7.76[30], which allows for the input of non-universal scalar and gaugino masses in gravity mediated SUSY breaking models where electroweak symmetry is broken radiatively. The relic density is evaluated via the IsaReD program[31], which is part of the Isatools package. IsaReD evaluates all $2 \rightarrow 2$ tree level neutralino annihilation and co-annihilation processes and implements relativistic thermal averaging in the relic density calculation.

In the upper frame of Fig. 3, we show the neutralino relic density for the parameter space point $m_0 = m_{1/2} = 300$ GeV, $A_0 = 0$, $\tan\beta = 10$ and $\mu > 0$, versus the ratio $r_2 = M_2(\text{GUT})/m_{1/2}$. For $r_2 = 1$ corresponding to the mSUGRA model, $\Omega_{\tilde{Z}_1} h^2 = 1.1$, so that the point is strongly excluded because it yields too much dark matter. For $r_2 \sim 0.6$, we arrive at the MWDM case explored in Ref. [16], while for $M_2 \sim -0.5$, we have BWCA,

explored in Ref. [18]. If we instead *increase* the magnitude of M_2 , then we find at $r_2 \sim 3$ a match to the measured relic abundance, with $\Omega_{\tilde{Z}_1} h^2 \sim 0.1$. This is the case of HM2DM. As we increase r_2 further, the relic density starts to go back up. This is because the neutralino mass falls below M_Z and ultimately M_W , so that (except neutralinos with high thermal energy) the processes $\tilde{Z}_1 \tilde{Z}_1 \rightarrow ZZ, WW$ become disallowed, and the total annihilation cross section is correspondingly reduced. Ultimately, the relic density again starts to drop because of the annihilation via off-shell Z . We note here that since the gaugino masses enter the soft SUSY breaking Higgs masses as their square, there is also a point with good relic density at $r_2 \sim -2.5$. Again, the shoulder in the relic density curve marks where the annihilation to vector boson pairs becomes disallowed.

$$m_0 = 300 \text{ GeV}, m_{1/2} = 300 \text{ GeV}, \tan\beta = 10, A_0 = 0, \mu > 0, m_t = 171.4 \text{ GeV}$$

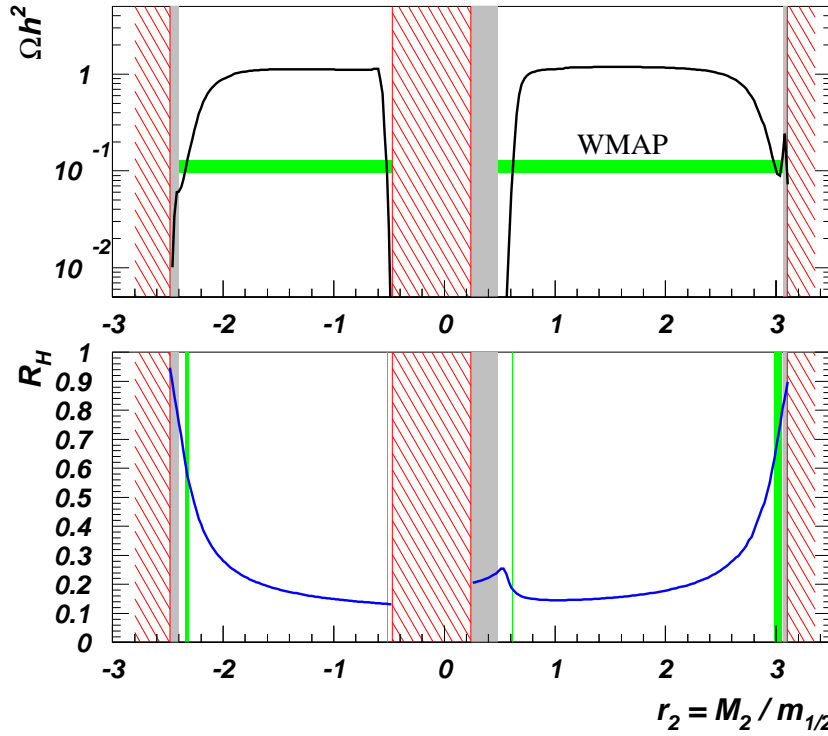


Figure 3: The neutralino relic density $\Omega_{CDM} h^2$ (upper frame) and the higgsino component $R_{\tilde{H}}$ of the lightest neutralino (lower frame) as a function of r_2 , for $m_0 = 300$ GeV, $m_{1/2} = 300$ GeV, $A_0 = 0$, $\tan\beta = 10$, $\mu > 0$ and $m_t = 171.4$ GeV. In the grey regions, the chargino mass falls below its lower limit of 103.5 GeV from LEP2 experiments, while the red hatched regions are excluded either because the Z width becomes too large, or because electroweak symmetry is not correctly broken. The green region is where the relic density falls in the range (1.1).

We also show the higgsino content of \tilde{Z}_1 , defined by $R_{\tilde{H}} \equiv \sqrt{v_1^{(1)2} + v_2^{(1)2}}$ (in the notation of Ref. [26]) in the lower frame of Fig. 3. We see that over the bulk of the range of r_2 , the higgsino composition of \tilde{Z}_1 is quite low, since \tilde{Z}_1 is dominantly bino-like, or for $0 \leq r_2 \leq 0.6$, a mixture of wino and bino. In the case of HM2DM with $r_2 \simeq 3$ or -2.5 , $R_{\tilde{H}}$ has risen to ~ 0.6 , indicating mixed higgsino-bino dark matter.

In Fig. 4, we show the thermally averaged neutralino annihilation cross section times relative velocity, integrated from temperature $x \equiv T/m_{\tilde{Z}_1} = 0$ to freeze-out $x = x_F$, versus r_2 for the same parameter choices as in Fig. 3. The inverse of this quantity enters the relic density calculation, so that a large integrated annihilation rate leads to a small relic density. For clarity, we display only positive values of r_2 . We see that while neutralino annihilation to lepton pairs via slepton exchange is dominant in the case of mSUGRA, when we move to the case of HM2DM, where the \tilde{Z}_1 is a mixed bino-higgsino state, then annihilation to WW , ZZ and Zh dominates, as is typical for mixed higgsino dark matter. As just discussed, these cross sections drop-off near the upper end of the range of r_2 once $m_{\tilde{Z}_1}$ falls below M_Z or M_W . In this range, annihilation via s -channel Z (which has large couplings to the \tilde{Z}_1 pair on account of the large higgsino content of \tilde{Z}_1) dominates, and ultimately becomes resonant so that the relic density drops below its observed value.

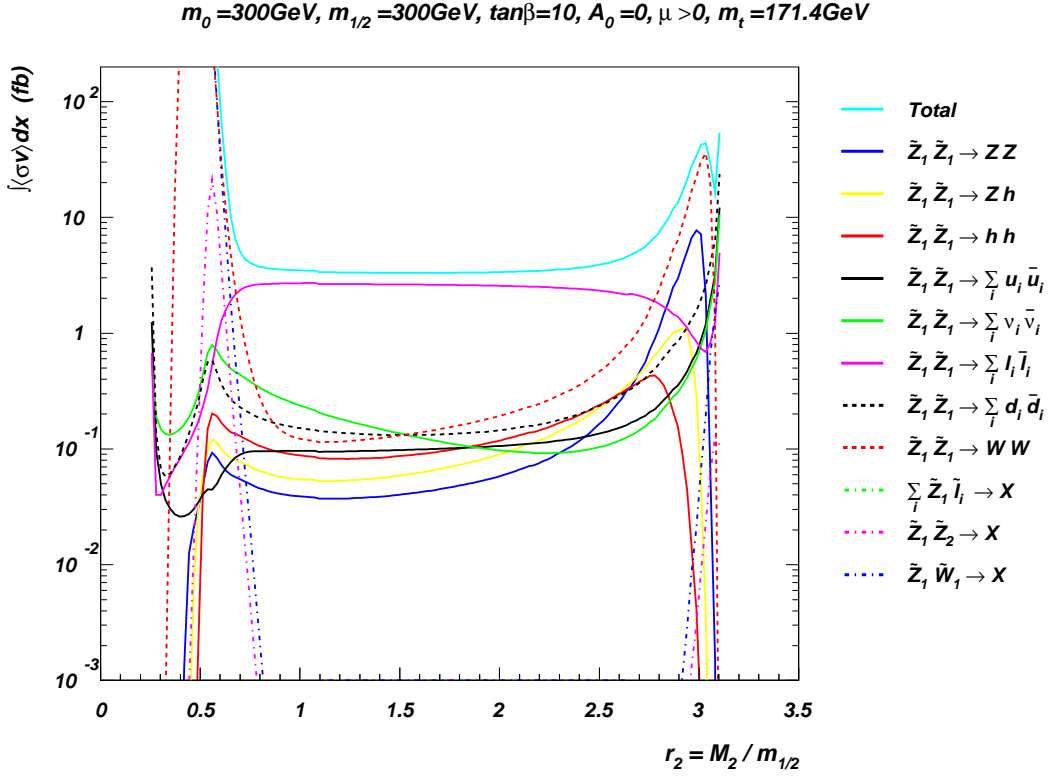


Figure 4: Thermally averaged neutralino annihilation cross sections (calculated in the HM2DM model) times neutralino relative velocity, integrated from $x = 0$ to x_F versus r_2 , for the same parameters as in Fig. 5.

In Fig. 5, we show the sparticle mass spectrum versus r_2 for the same parameter choice as in Fig. 3. At $r_2 = 1$, we see a large mass gap $m_{\tilde{Z}_2} - m_{\tilde{Z}_1} \sim 100$ GeV in the case of the mSUGRA model. As M_2 increases, the μ parameter decreases, and falls rapidly beyond $r_2 \sim 2$. In the region of $r_2 \sim 2.5 - 3$, the curves for $m_{\tilde{Z}_2}$, $m_{\tilde{Z}_3}$ and $m_{\tilde{W}_1}$, and for very large r_2 , $m_{\tilde{Z}_1}$ in place of $m_{\tilde{Z}_3}$, track the μ value, indicating that these particles are dominantly higgsino-like. We also see that $m_{\tilde{e}_L}$, and $m_{\tilde{u}_L, \tilde{d}_L}$ all increase with increasing r_2 ,

$m_0=300\text{GeV}, m_{1/2}=300\text{GeV}, \tan\beta=10, A_0=0, \mu > 0, m_t=171.4\text{GeV}$

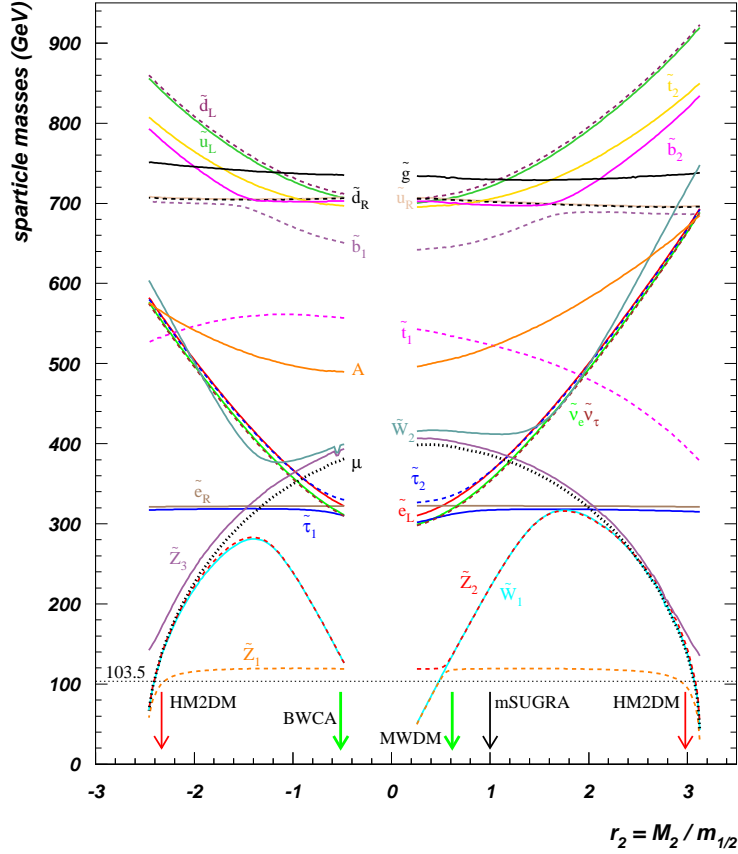


Figure 5: Various sparticle and Higgs boson masses and the μ parameter in the HM2DM model versus r_2 for $m_0 = 300$ GeV, $m_{1/2} = 300$ GeV, $A_0 = 0$, $\tan\beta = 10$ and $\mu > 0$.

owing to the upward push in their respective RGEs. The value of m_A , given at tree-level by $m_A^2 \sim m_{H_d}^2 - m_{H_u}^2$, also increases with r_2 as can be seen from Fig. 1a. The right- squark and slepton masses, on the other hand, are roughly independent of r_2 , so that in HM2DM we expect a larger mass gap between L and R squarks and sleptons relative to the mSUGRA model. This also leads to the level-crossing in the b -squark system that we mentioned earlier: for small values of r_2 (including in the mSUGRA model) \tilde{b}_1 is dominantly \tilde{b}_L , while for $r_2 \gtrsim 2$, \tilde{b}_1 becomes mostly \tilde{b}_R . The value of $m_{\tilde{t}_1}$ actually decreases with increasing M_2 , which is due in part to the diminishing value of $m_{\tilde{t}_R}^2$ as shown in Fig. 2a), and in part due to an increasingly negative weak scale value of A_t . For the most part, the figure is nearly symmetric between positive and negative values of M_2 since, as mentioned above, the scalar SSB RGEs contain M_2^2 , and not M_2 . The $A_{t,b,\tau}$ parameter RGEs all have M_2 entering linearly, so that A term evolution is *not* symmetric between positive and negative μ . This gives rise to the unsymmetrical behavior, most noticeable in the $m_{\tilde{t}_1}$ curve. Of course, $m_{\tilde{W}_2}$ – which becomes essentially $|M_2|$ in the HM2DM model – is also asymmetric since the value of $|r_2|$ required to saturate the relic density is itself asymmetric between

positive and negative masses. This asymmetry could have an impact upon the accessibility of \tilde{W}_2 and \tilde{Z}_4 at future electron-positron colliders.

We have already discussed how the intra-generation mixing patterns are affected by the large value of $|M_2|$: since a large value of $m_{f_L}^2$ results when $|M_2|$ is large, the lighter sfermions are dominantly \tilde{f}_R within the HM2DM framework. This is confirmed in Fig. 6, where we show the dependence of the sfermion mixing angle θ_f defined in Ref. [26] on r_2 for the same parameters as in Fig. 5. We see that the \tilde{b}_1 and $\tilde{\tau}_1$ are essentially \tilde{b}_R and $\tilde{\tau}_R$ in the HM2DM model.

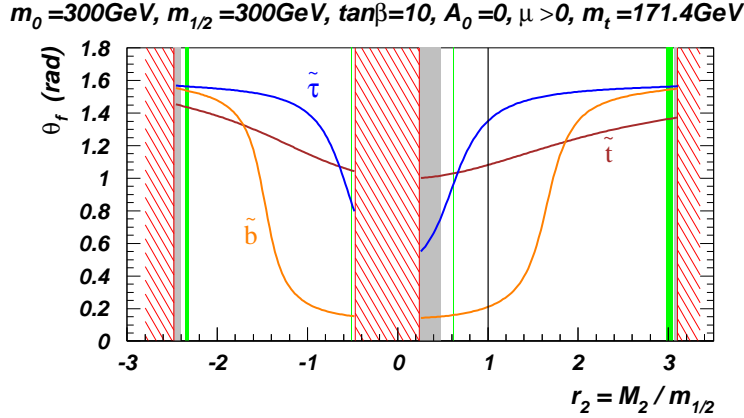


Figure 6: The sfermion mixing angle θ_f as defined in Ref.[26] for $f = t, b$ and τ versus r_2 for $m_0 = 300$ GeV, $m_{1/2} = 300$ GeV, $A_0 = 0$, $\tan\beta = 10$ and $\mu > 0$. We see that for the HM2DM model, the θ_f are all large so that the lighter states are all dominantly right sfermions. The various shadings are the same as in Fig. 3.

In Table 1, we list various sparticle masses and μ , along with expectations for the relic density, a_μ^{SUSY} , $BF(b \rightarrow s\gamma)$ and spin-independent direct DM detection cross section $\sigma_{SI}(\tilde{Z}_1 p)$ for several different cases with all parameters other than $M_2(\text{GUT})$ set as in Fig. 5. The first case, mSUGRA, provides a benchmark for comparison with the HM2DM cases. For case HM2DM1, we take $M_2 = 900$ GeV, to obtain $\Omega_{\tilde{Z}_1} h^2 \sim 0.1$ as required by observation. As expected the gluino mass hardly changes in going from mSUGRA to HM2DM1, while the light charginos and neutralinos have all gotten much lighter in accord with the decreasing μ parameter. The light chargino also changes its character from being dominantly wino-like to dominantly higgsino-like. In fact, the mass gap $m_{\tilde{Z}_2} - m_{\tilde{Z}_1}$, which was of order 100 GeV in mSUGRA, has dropped to ~ 50 GeV in HM2DM1. This means the spoiler decay modes $\tilde{Z}_2 \rightarrow \tilde{Z}_1 h$ and $\tilde{Z}_2 \rightarrow \tilde{Z}_1 Z$ will be closed for HM2DM, and a dilepton mass edge should be visible in collider events where \tilde{Z}_2 is produced at large rates either directly or via gluino and squark cascade decays. The neutralino \tilde{Z}_3 also has a large higgsino component and cannot be split very much from \tilde{Z}_2 ; its leptonic decays, therefore, should also lead to a distinct mass edge in the dilepton mass spectrum. We also note that the left- squarks and sleptons have become 200-300 GeV heavier than in mSUGRA, while the masses of right- squarks and sleptons, as expected in the HM2DM scenario, are essentially unchanged. The top squark \tilde{t}_1 has become significantly lighter in the HM2DM1

parameter	mSUGRA	HM2DM1	HM2DM2	HM2DM3
m_0	300	300	300	300
M_1	300	300	300	300
M_2	300	900	-700	-695
M_3	300	300	300	300
μ	385.1	134.8	136.5	-144.4
$m_{\tilde{g}}$	729.7	736.4	749.7	749.5
$m_{\tilde{u}_L}$	720.8	901.8	840.7	838.6
$m_{\tilde{t}_1}$	523.4	394.3	533.0	534.7
$m_{\tilde{b}_1}$	656.8	686.4	701.2	700.7
$m_{\tilde{e}_L}$	364.5	669.3	559.9	557.0
$m_{\tilde{e}_R}$	322.3	321.3	321.4	321.4
$m_{\tilde{W}_2}$	411.7	719.7	575.7	575.1
$m_{\tilde{W}_1}$	220.7	136.5	133.9	144.4
$m_{\tilde{Z}_4}$	412.5	723.1	583.2	580.7
$m_{\tilde{Z}_3}$	391.3	160.2	170.1	168.4
$m_{\tilde{Z}_2}$	220.6	142.3	136.2	141.9
$m_{\tilde{Z}_1}$	119.2	94.8	99.9	108.6
m_A	520.3	670.7	565.0	563.3
m_{H^+}	529.8	679.8	574.3	572.7
m_h	110.1	111.9	107.6	107.5
$\Omega_{\tilde{Z}_1} h^2$	1.1	0.10	0.11	0.12
$BF(b \rightarrow s\gamma)$	3.0×10^{-4}	2.3×10^{-4}	3.3×10^{-4}	4.0×10^{-4}
Δa_μ	12.1×10^{-10}	3.1×10^{-10}	-7.4×10^{-10}	7.0×10^{-10}
$\sigma_{SI}(\tilde{Z}_1 p)$	2.1×10^{-9} pb	3.4×10^{-8} pb	2.5×10^{-8} pb	3.2×10^{-9} pb
$ v_1^{(1)} $	0.05	0.40	0.37	0.32

Table 1: Input parameters and resultant sparticle masses in GeV units together with the predicted neutralino relic density, direct LSP detection scattering cross section from a proton, $B(b \rightarrow s\gamma)$ and Δa_μ , the SUSY contribution to the anomalous magnetic moment of the muon, for mSUGRA and three HM2DM scenarios. In each case, we fix $A_0 = 0$, $\tan\beta = 10$ and $m_t = 171.4$ GeV.

case, which leads to a deviation of the branching fraction $B(b \rightarrow s\gamma)$ from its SM value. In contrast, the SUSY contribution to Δa_μ is diminished, owing to the increased left smuon and sneutrino masses. The DM direct detection rate has increased to the $\sim 10^{-8}$ pb level expected in models with MHDM [22]. In case HM2DM2, we take $M_2 = -700$ GeV, which also gives the correct relic abundance. In this case, the \tilde{t}_1 is heavier than in case HM2DM1, so that $BF(b \rightarrow s\gamma)$ is more closely in agreement with its measured value: $BF(b \rightarrow s\gamma) = (3.55 \pm 0.26) \times 10^{-4}$ from a combination of CLEO, Belle and BABAR data[32]. However, the value of Δa_μ^{SUSY} , which is proportional to $\frac{m_\mu^2 \mu M_2 \tan\beta}{M_{SUSY}^4}$, has turned negative, in contrast to the measured deviation, which is positive. This can be rectified by choosing in addition to $M_2 < 0$, $\mu < 0$, as in the HM2DM3 case in the last column of the table. This case now gives a positive contribution to Δa_μ , but also a deviation in

$BF(b \rightarrow s\gamma)$ which is now somewhat larger than the measured value. This latter case with opposite signs of μ and M_1 also gives a significantly lower direct DM detection cross section, due to negative interference between h - and H -mediated scattering amplitudes [33, 34].

While our discussion up to now has been confined to particular values of $m_0, m_{1/2}, \dots$, it should be clear that the method of raising $|M_2|$ to obtain MHDM in agreement with (1.1) is quite general, although a different value of $|r_2|$ will be needed for each point in m_0 vs. $m_{1/2}$ parameter space. We have scanned over the m_0 vs. $m_{1/2}$ parameter space for $A_0 = 0$ and $\tan\beta = 10$ to extract the particular r_2 value needed at each point to obtain the WMAP measured CDM density. The results are shown as contours of r_2 in Fig. 7 for a) $M_2 > 0$ with $\mu > 0$, and b) $M_2 < 0$ with $\mu < 0$. The red-shaded regions are theoretically excluded, due to lack of EWSB, due to a stau or (if r_2 is very small) chargino LSP, or because the Z -width constraint is violated. The blue shaded regions are excluded because $m_{\tilde{W}_1} < 103.5$ GeV, in contradiction with sparticle search limits from LEP2. The green shaded regions give $\Omega_{\tilde{Z}_1} h^2 < 0.13$ in the mSUGRA model, so in these regions there is no need to dial M_2 to large values. In frame a), the contours in r_2 range from $r_2 \sim 3$ in the low $m_0, m_{1/2}$ region, to $r_2 \lesssim 2$ when nearing the HB/FP region (which already has $|\mu|$ suppression due to a large m_0 value). We note the appearance of a white region to the left of the mSUGRA stau co-annihilation region that is allowed in the HM2DM framework; in this case, since $|\mu|$ is reduced, the value of $m_{\tilde{Z}_1} \sim |\mu|$ and falls below $m_{\tilde{\tau}_1}$. There is also a region just below $m_{1/2} \sim 0.3$ TeV which turns out to be LEP2 excluded, while even smaller values of $m_{1/2} \sim 0.2$ TeV re-emerge as LEP2 allowed. The LEP2 excluded region at $m_{1/2} \sim 225 - 290$ GeV occurs because for $m_{1/2} < 290$ GeV, $m_{\tilde{Z}_1}$ drops first below M_Z , then below M_W . This shuts off the $\tilde{Z}_1 \tilde{Z}_1 \rightarrow ZZ, WW$ annihilation modes, so that even larger M_2 values are needed to drive $|\mu|$ to even smaller values. The lower $|\mu|$ values then drive $m_{\tilde{W}_1}$ below the LEP2 search limit that requires $m_{\tilde{W}_1} > 103.5$ GeV. For even lower $m_{1/2}$ values, the allowed region opens up again because, for the smaller value of $m_{1/2}$, the higgsino components of \tilde{Z}_1 allow for efficient annihilation through the *off-shell* s -channel Z exchange so $|\mu|$ need not be as small, and the chargino mass can be above the LEP2 bound in the range of $m_{1/2} \sim 150$ -225 GeV.

The corresponding contours for negative M_2 are shown in Fig. 7b), where we also take $\mu < 0$ to realize a positive value of $\Delta a_\mu^{\text{SUSY}}$; the frame mainly differs from the positive M_2 case in that the range of $|r_2|$ is somewhat lower than in frame a), presumably because of differences in $m_{\tilde{Z}_1}$ and in the coupling of \tilde{Z}_1 to W 's and Z 's. The LEP2-allowed region at $m_{1/2} \sim 0.2$ TeV from frame a) now also disappears (despite the smaller value of r_2 , μ is now slightly smaller than in frame a, making it more difficult to evade the LEP 2 bound), except for the thin sliver where $2m_{\tilde{Z}_1} \sim m_h$ where, because of the resonance enhancement, a raised value of M_2 is not needed to saturate the measured relic density.

Up to now, we have confined our discussion to a fixed value of $\tan\beta = 10$. Our considerations also apply for other values of $\tan\beta$. Specifically, we have checked that for $m_0 = m_{1/2} = 300$ GeV, $A_0 = 0$ and $\mu > 0$, that the relic density measurement is saturated for $r_2 : 2.8 - 3.4$ for $\tan\beta \lesssim 40$; for yet larger values of $\tan\beta$, the required value of r_2 drops rapidly, and consistency with the upper bound on the relic density is possible in the

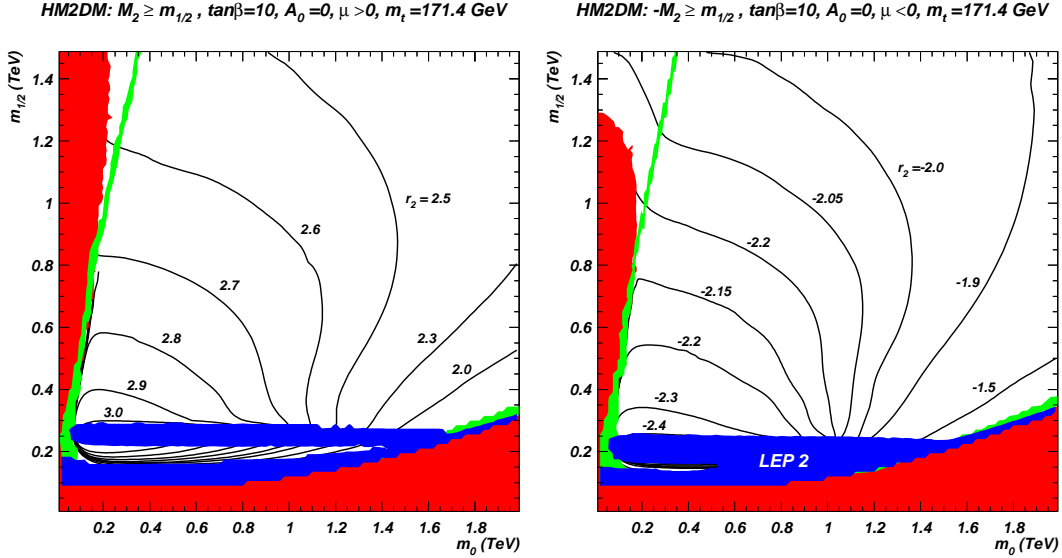


Figure 7: Contours of r_2 in the m_0 vs. $m_{1/2}$ plane with $\tan\beta = 10$, $A_0 = 0$ for a) $M_2 > 0$ with $\mu > 0$, and b) $M_2 < 0$ with $\mu < 0$. Each point in these planes has r_2 dialed to a high value such a value that $\Omega_{\tilde{Z}_1} h^2 \simeq 0.11$. The red and blue regions are excluded for reasons explained in the text.

mSUGRA model once $\tan\beta \gtrsim 46$ because neutralino annihilation via s -channel A becomes large, while for the largest values of $\tan\beta$ co-annihilation via staus becomes dominant.

3. $b \rightarrow s\gamma$ and $(g - 2)_\mu$

Now that we have established that any point in m_0 vs. $m_{1/2}$ space can be made dark-matter consistent by increasing $|M_2|$, we delineate regions of parameter space where the recent measurements of the branching fraction $BF(b \rightarrow s\gamma)$ [32] or of $(g - 2)_\mu$ [35, 36] are consistent with predictions of the HM2DM model.

3.1 $BF(b \rightarrow s\gamma)$

The branching fraction $BF(b \rightarrow s\gamma)$ is extremely interesting largely because amplitudes for supersymmetric contributions mediated by $\tilde{W}_i \tilde{t}_j$ and bH^+ loops are expected to be of similar size as the leading SM amplitude mediated by a tW loop [37]. The measured branching fraction, from a combination of CLEO, Belle and BABAR experiments [32], is $BF(b \rightarrow s\gamma) = (3.55 \pm 0.26) \times 10^{-4}$, while the latest SM calculations find [38] $BF(b \rightarrow s\gamma) = (3.29 \pm 0.33) \times 10^{-4}$. In view of the good agreement between the SM and experiment, any SUSY contribution to $BF(b \rightarrow s\gamma)$ should be somewhat suppressed, unless there are cancellations between different SUSY loops, or the summed SUSY contribution fortuitously turns out to be twice the SM amplitude but with the opposite sign.

We evaluate $BF(b \rightarrow s\gamma)$ using the IsaBSG code [37], a part of the Isatools package. The dependence of the branching fraction on r_2 is illustrated in Fig. 8 for our canonical point 1 from Table 1. We see that in the mSUGRA case, $BF(b \rightarrow s\gamma)$ is not far below its measured value. Dialing r_2 to high positive values decreases the branching fraction

(recall that \tilde{t}_1 becomes lighter) and the discrepancy with experiment grows until we hit the green DM allowed region, where we find $BF(b \rightarrow s\gamma) \sim 2.3 \times 10^{-4}$. For negative values of r_2 , $BF(b \rightarrow s\gamma)$ varies much less, and in the WMAP-favoured range is actually in close accord with its measured value. For the favoured negative sign of μ , the branching fraction becomes a bit too large when $r_2 < 0$.

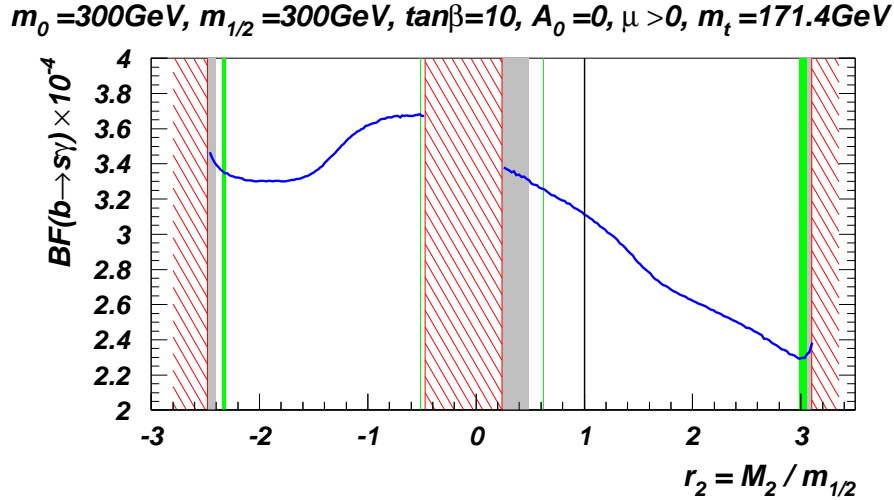


Figure 8: Branching fraction $BF(b \rightarrow s\gamma)$ versus M_2 for $m_0 = m_{1/2} = 300$ GeV, $A_0 = 0$, $\tan\beta = 10$, and $\mu > 0$. The various shadings are the same as in Fig. 3.

While this particular point at high $M_2 > 0$ may seem somewhat discouraging, in Fig. 9 we show by the black contours the branching fraction $BF(b \rightarrow s\gamma)$ in the m_0 vs. $m_{1/2}$ plane with $A_0 = 0$, $\tan\beta = 10$ and a) $M_2 > 0$ with $\mu > 0$, and b) $M_2 < 0$ with $\mu < 0$, where at each point we have dialed $|M_2|$ to high values so that that $\Omega_{\tilde{Z}_1} h^2$ saturates the measured value in (1.1). In frame a), we see that $BF(b \rightarrow s\gamma)$ is low only in the very low m_0 and $m_{1/2}$ corner, but is not far from its measured value (considering theoretical uncertainties) for $m_0, m_{1/2} \gtrsim 0.5$ TeV. In contrast, in frame b), the measured value of $BF(b \rightarrow s\gamma)$ clearly disfavors small values of m_0 and $m_{1/2}$, requiring these to be $\gtrsim 700$ GeV.

3.2 $(g - 2)_\mu$

Current measurements of the muon anomalous magnetic moment show an apparent deviation from SM predictions. Combining QED, electroweak, hadronic (using $e^+e^- \rightarrow$ hadrons to evaluate hadronic loop contributions) and light-by-light contributions, and comparing against measurements from E821 at BNL, a *positive* deviation in $a_\mu \equiv \frac{(g-2)_\mu}{2}$ of

$$\Delta a_\mu = a_\mu^{exp} - a_\mu^{SM} = 22(10) \times 10^{-10} \quad (3.1)$$

is reported in the Particle Data Book[35], *i.e.* a 2.2σ effect.⁴

⁴More recent analyses[36] report a larger discrepancy if only electron-positron data are used for the evaluation of the hadronic vacuum polarization contribution; the significance of the discrepancy is, however, reduced if tau decay data are used for this purpose.

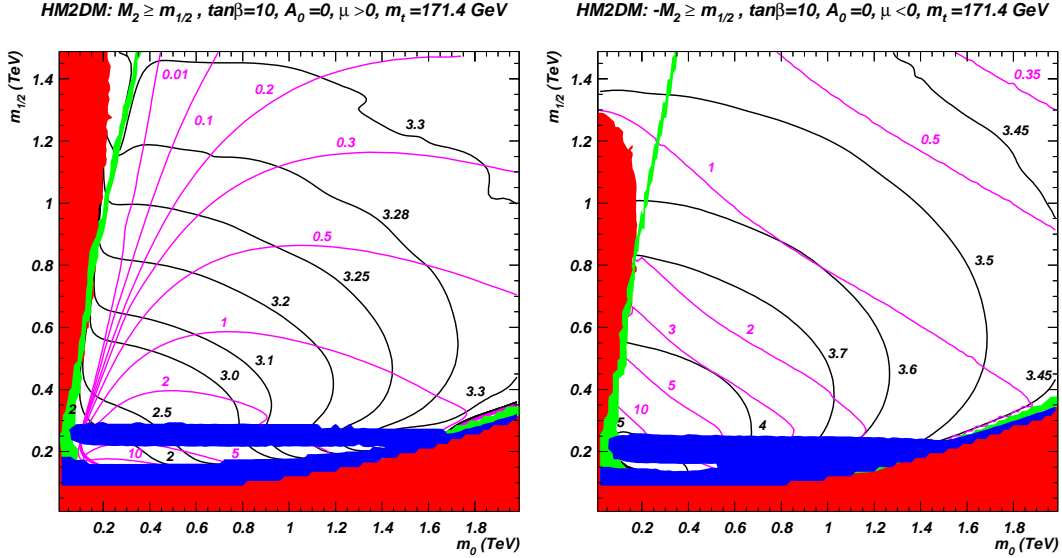


Figure 9: Contours of branching fraction $BF(b \rightarrow s\gamma) \times 10^4$ (black) and $\Delta a_\mu \times 10^{10}$ (purple) in the m_0 vs. $m_{1/2}$ plane for $A_0 = 0$, $\tan\beta = 10$, and a) $r_2 > 0$ with $\mu > 0$, and b) $r_2 < 0$ with $\mu < 0$ where M_2 has been dialed at every point to large values such that $\Omega_{\tilde{Z}_1} h^2 \sim 0.1$.

One-loop diagrams with $\tilde{W}_i - \tilde{\nu}_\mu$ and $\tilde{Z}_i - \tilde{\mu}_{1,2}$ in the loop would give supersymmetric contributions to a_μ , perhaps accounting for the (rather weak, yet persistent) discrepancy with the SM. For our canonical point with $m_0 = m_{1/2} = 300$ GeV, we have checked that even though $|M_2|$ is large, the *total* chargino contribution to Δa_μ dominates the *total* neutralino contribution even in the HM2DM model exactly as in the mSUGRA case. This is the case for both signs of M_2 . For $M_2 > 0$ the total neutralino contribution, though much smaller than the corresponding chargino contribution, is relatively larger in the HM2DM case as compared with mSUGRA.

The purple curves in Fig. 9 are contours of $\Delta a_\mu^{\text{SUSY}} \times 10^{10}$ in the m_0 vs. $m_{1/2}$ plane. For $M_2 > 0$ shown in frame a), in the portion of the plane not strongly excluded by the $b \rightarrow s\gamma$ constraint, we see that model, $\Delta a_\mu^{\text{SUSY}}$ is very small. The situation for $M_2 < 0$ is very similar as can be seen from frame b). While it appears that the HM2DM model will be strongly disfavoured if the muon magnetic moment discrepancy continues to persist, we should remember that (1) $\Delta a_\mu^{\text{SUSY}}$ and $BF(b \rightarrow s\gamma)$ are both sensitive to $\tan\beta$, and (2) the latter is very sensitive to small flavour violations in the soft-SUSY breaking parameters which will not have any significant effect on direct searches for supersymmetry.

4. Direct and indirect detection of neutralino CDM

In this section, we explore the prospects for direct and indirect detection of neutralino dark matter within the HM2DM framework[39]. We adopt the IsaReS code[40] (a part of the Isatools package) for the computation of the direct detection rates and the DarkSUSY code [41], interfaced to Isajet, for the computation of the various indirect detection rates. Indirect detection rates are sensitive to the DM distribution in our galactic halo, larger

rates being obtained for a clumpy or cuspy halo distribution as compared with a smooth or less peaked distribution of the DM. We show our results for two halo profiles. The Adiabatically Contracted N03 Halo model[42], where the deepening of the gravitational potential wells caused by baryon in-fall leads to a higher concentration of DM in the center of the the Milky Way, gives higher detection rates, especially for gamma ray and anti-particle detection than smoother halo profiles. For comparison, we also show projections using the Burkert profile[43] where the central cusp in the DM halo is smoothed out by significant heating of cold particles.⁵ In our analysis, we consider signals from the following processes.

1. Relic neutralinos in our galactic halo can scatter from nuclei in the material of underground cryogenic or noble liquid detectors designed to detect the resulting nuclear recoil, leading to direct detection of the neutralino [46]. Although there is no positive signal to date, the most stringent upper limit on the scattering cross section comes from the XENON-10 collaboration [47], which obtained an upper limit $\sigma(\tilde{Z}_1 p) \lesssim 8 \times 10^{-8}$ pb for $m_{\tilde{Z}_1} \sim 100$ GeV, corresponding to the expected neutralino mass in the HM2DM model for our canonical choice of parameters in Fig. 1. We compute the spin independent neutralino-proton scattering cross section (used as the figure of merit in these experiments), and compare it to projections for the sensitivity of Stage 2 detectors (CDMS2[48], Edelweiss2[49], CRESST2[50], ZEPLIN2[51]) which are expected to probe a factor of ~ 5 below the XENON-10 bound.⁶

We also compare expectations in the HM2DM model with the projected sensitivity of the proposed SuperCDMS detector with 25 kg of Ge, and with proposed ton-size noble liquid detectors (XENON[53], LUX, WARP[54] and CLEAN[55]), for which we use the sensitivity of Warm Argon Project, with 1400 kg of argon as the benchmark.

2. Neutralinos gravitationally trapped in the core of the sun may be indirectly detected via their annihilation to neutrinos at neutrino telescopes [56]. Here, we present rates for detection of $\nu_\mu \rightarrow \mu$ conversions at Antares[57] or IceCube[58]. The reference experimental level we use is the ultimate sensitivity of IceCube, with a muon energy threshold of 50 GeV, corresponding to a flux of about 40 muons per km² per year.
3. Indirect detection of neutralinos may also be accomplished by detection of high energy gamma rays from neutralino annihilation in the galactic center. Such gamma rays[59] have already been detected by EGRET[60], and will be searched for by the GLAST experiment[61]. We evaluate the integrated continuum γ ray flux above a $E_\gamma = 1$ GeV threshold, and take the GLAST sensitivity of 1.0×10^{-10} cm⁻²s⁻¹ as our benchmark.
4. Indirect detection of neutralinos is also possible via the detection of anti-particles from neutralino annihilations in the galactic halo. Proposed and on-going experiments include searches for positrons[62] (HEAT[63], Pamela[64] and AMS-02[65]),

⁵For a comparison of the implications of different halo model choices for indirect DM detection rates, see *e.g.* Refs. [44, 34, 45, 14].

⁶In our analysis, we took the π -nucleon Σ term to be 45 MeV. Different values recently suggested by other groups can change our predictions by about factor of three [52].

antiprotons[66] (BESS[67], Pamela, AMS-02) and anti-deuterons (\bar{D}) (BESS[68], AMS-02, GAPS[69]). For positrons and antiprotons we evaluate the averaged differential antiparticle flux in a projected energy bin centered at a kinetic energy of 20 GeV, where we expect an optimal statistics and signal-to-background ratio at space-borne antiparticle detectors[45, 70]. We take the experimental sensitivity to be that of the Pamela experiment after three years of data-taking as our benchmark. Finally, we evaluate the average differential anti-deuteron flux in the $0.1 < T_{\bar{D}} < 0.25$ GeV range, where $T_{\bar{D}}$ stands for the anti-deuteron kinetic energy per nucleon, and compare it to the estimated GAPS sensitivity for an ultra-long duration balloon-borne experiment [69] (see Ref. [71] for an updated discussion of the role of antideuteron searches in DM indirect detection).

In Fig. 10, we illustrate the various direct and indirect DM detection rates for our canonical case with $m_0 = m_{1/2} = 300$ GeV, $A_0 = 0$, $\tan\beta = 10$ and $\mu > 0$, where M_2 is allowed to vary. The M_2 value corresponding to the mSUGRA model is denoted by a solid black vertical line at $r_2 = 1$, while the HM2DM scenarios for $r_2 < 0$ and $r_2 > 0$ with $\Omega_{\tilde{Z}_1} h^2$ within the WMAP range (1.1) are shown by the green regions on the left and right ends of the plot. The MWDM and BWCA solutions are seen as the very narrow green regions near $r_2 \sim \pm(0.5 - 0.6)$. The dotted lines correspond to the sensitivity level for representative searches: *i.e.*, the signal is observable only when the model prediction is higher than the corresponding dotted line.

In frame *a*), we show the spin-independent neutralino-proton scattering cross section. We see that for a bino-like neutralino with $m_{\tilde{Z}_1} \sim 100$ GeV as in the mSUGRA or BWCA cases, the signal will only be detectable if the cross section can be probed at the 10^{-9} pb level as envisioned at superCDMS or at 100-1000 kg noble liquid detectors. In contrast, in both the HM2DM regions where the neutralino has a significant higgsino component, the cross section is just below the current bound, and should be detectable at CDMS2. This is simply a reflection of the well-known result that MHDM has rather large neutralino-proton scattering rates, as is typified by the HB/FP region of the mSUGRA model, and further, that experimental sensitivity at the 10^{-8} pb level will probe a wide class of models with MHDM [22].

In Fig. 11, we show the expected value of $\sigma_{SI}(\tilde{Z}_1 p)$ in the HM2DM model, resulting from a scan in m_0 and $m_{1/2}$, keeping $\tan\beta = 10$ and $A_0 = 0$, and where we adjust M_2 to get agreement with (1.1), for $M_2 > 0$ with $\mu > 0$ (upper frame) and $M_2 < 0$ with $\mu < 0$ (lower frame). Also shown are the sensitivity limits for CDMS2, superCDMS and WARP 1400 kg. The most striking feature of the figure is that the bulk of the points in the scan give a cross section around 10^{-8} pb, independent of the neutralino mass. This is because the increased bino-higgsino mixing necessary to maintain agreement with (1.1) for larger values of $m_{\tilde{Z}_1}$ compensates for the drop in cross section for larger neutralino masses. We also see that the cross sections for negative M_2 are systematically lower than those for $M_2 > 0$. We have checked that flipping the relative sign between M_1 and μ causes a flip in the relative sign between the $h\tilde{Z}_1\tilde{Z}_1$ coupling and the $H\tilde{Z}_1\tilde{Z}_1$ coupling, so that h - and H -mediated amplitudes for neutralino-nucleon scattering interfere constructively

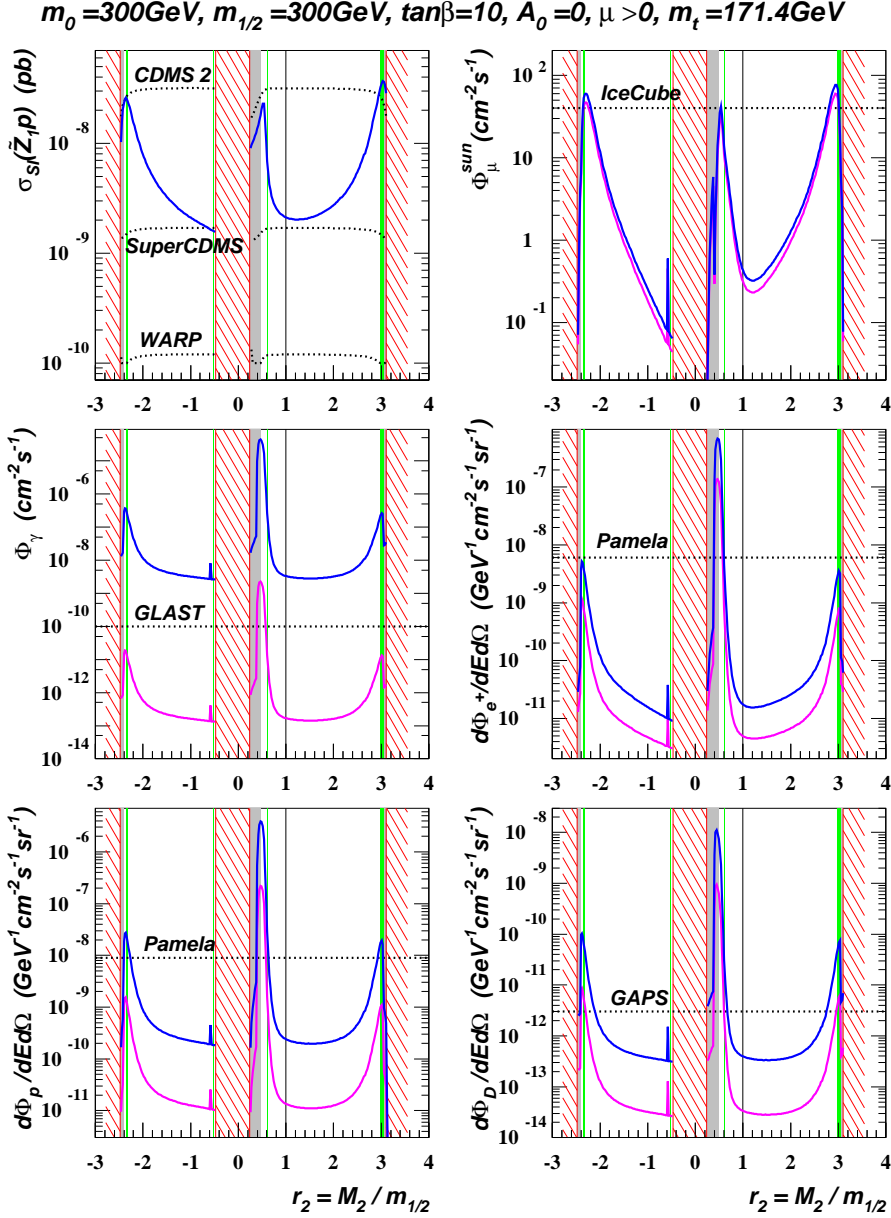


Figure 10: Rates for direct and indirect detection of neutralino dark matter *vs.* r_2 for $m_0 = m_{1/2} = 300 \text{ GeV}$, with $\tan\beta = 10$, $A_0 = 0$, $\mu > 0$. The various shadings are the same as in Fig. 3. The blue curves correspond to the Adiabatically Contracted N03 dark matter halo model, while the purple ones are for the Burkert profile. For each experiment, the signal is observable if the rate is above the corresponding dotted curve.

in the positive μ case and destructively for negative μ , accounting for the drop in the cross section. (Since squarks are heavy, squark-mediated amplitudes are negligible.)⁷ The

⁷In more detail, the flip of the sign of μ flips the relative sign between the up- and down- higgsino components in \tilde{Z}_1 . Further, since $m_A \gg M_{\text{weak}}$ for the HM2DM model, the Higgs mixing angle satisfies $\tan\alpha \simeq \cot\beta$, so that for $\tan\beta \gtrsim 10$, $\text{Re}h_u^0 \sim h$ and $\text{Re}h_d^0 \sim H$. As a result, there is a flip of the relative

cluster of points below $m_{\tilde{Z}_1} = 100$ GeV in the upper frame are points in the white strip at $m_{1/2} \sim 0.2$ TeV inside the blue region in Fig. 7a). We see that while superCDMS should probe all the points for positive values of M_2 , the increased sensitivity of ton-size noble element detectors appears essential in the $M_2 < 0$ case.

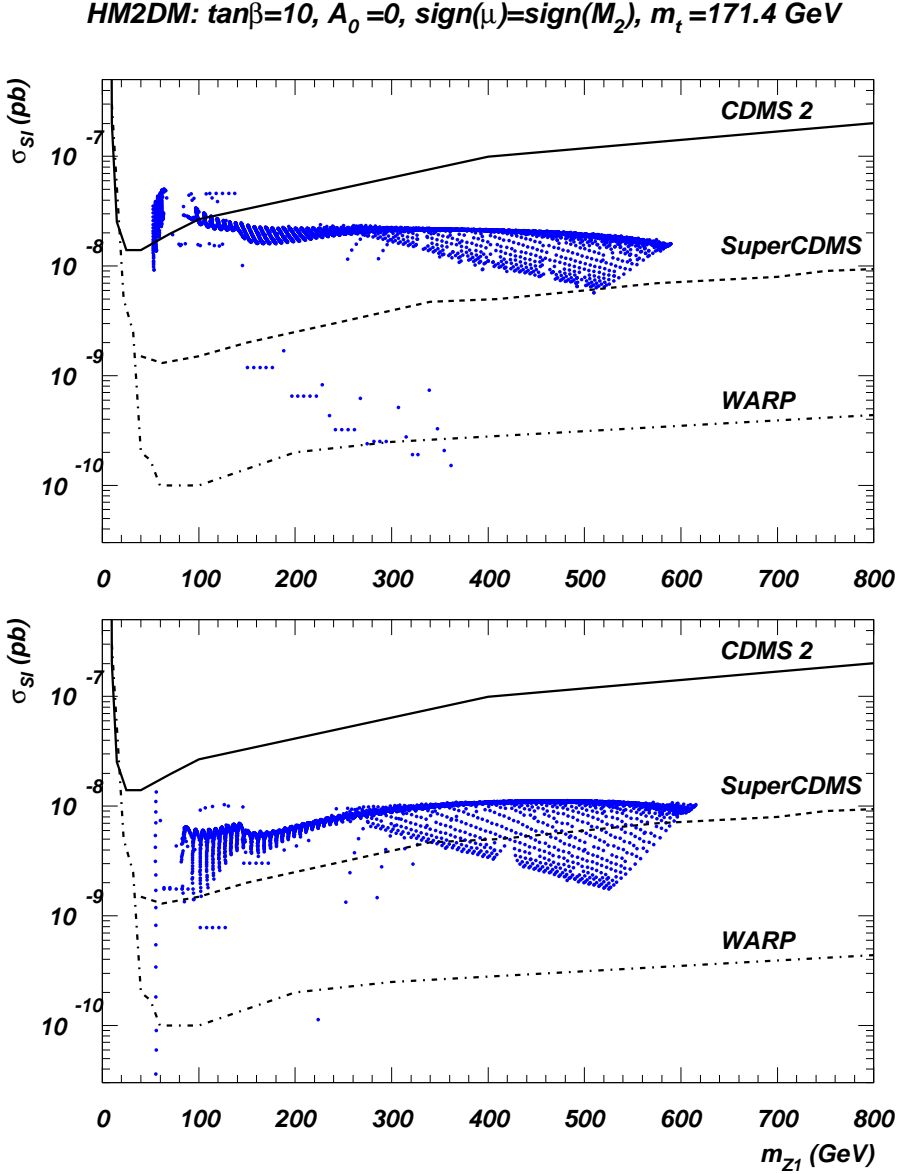


Figure 11: The neutralino-proton scattering cross section for the HM2DM model with $\tan\beta = 10$ and $A_0 = 0$, but where we scan over m_0 and $m_{1/2}$ for $M_2 > 0$ with $\mu > 0$ (upper frame), and $M_2 < 0$ with $\mu < 0$ (lower frame). For each point on this plot, M_2 is adjusted to saturate the observed DM density. We retain only those points where $m_{\tilde{W}_1} \geq 103.5$ GeV in this plot.

Turning to indirect dark matter detection, in Fig. 10b), we show the flux of muons

 sign between the $\tilde{Z}_1\tilde{Z}_1h$ and $\tilde{Z}_1\tilde{Z}_1H$ couplings.

from neutralino pair annihilations in the core of the Sun, again for our canonical choice of parameters introduced in Fig. 1. The blue and purple curves are our projections assuming the Adiabatically Contracted N03 Halo model[42] and the Burkert profile[43], respectively, for the distribution of DM in our galaxy. In this case, the result is only mildly sensitive to the choice of halo distribution, since the muon flux is mainly determined by the equilibrium density of neutralinos in the sun, and the cross section for neutralino annihilation into neutrinos. We see that the expected muon flux is more than an order of magnitude below the projected sensitivity of IceCube in the mSUGRA framework, but is larger by over two orders of magnitude, and in the observable range, for the HM2DM model on account of the increased higgsino content of the LSP. The muon flux rapidly drops off near the ends where $m_{\tilde{Z}_1}$ falls below M_W because the neutrinos (which then mainly come from decays of heavy quarks) become very soft, so that their efficiency for detection at IceCube is vastly degraded.

In frames *c*), *d*), *e*) and *f*) we show the flux of photons, positrons, antiprotons and antideuterons, respectively. Also shown by the horizontal lines are the anticipated experimental sensitivities. Again, we show results using the Adiabatically Contracted N03 Halo model (blue) and the Burkert profile (purple). We see that the projections are sensitive to the assumed halo distribution. This is most striking for the photon signal at GLAST, where the difference is more than four orders of magnitude. This is because most of the photons come from the galactic center where the difference between the two profiles is the most pronounced. In contrast, projections for the detection of positrons, anti-protons and anti-deuterons from neutralino annihilation (unlike photons, these can reach the earth only from limited distances) differ by a factor of 5-15. Again, the rates for indirect detection via observation of halo annihilation remnants, which are typically low for bino-like DM as in the mSUGRA model, jump by a factor of 30-300 in the HM2DM model where $|r_2|$ is increased so that the measured CDM relic abundance is obtained. For our choice of model parameters, the GAPS experiment should be able to detect anti-deuterons even for the case of the Burkert halo profile, while the positron signal in Pamela is projected to be just below its sensitivity limit even for the optimistic N03 Halo profile. The situation for the anti-proton signal is less conclusive since its detectability clearly depends on the halo distribution.

5. Supersymmetry signals at colliders

We now turn to an examination of the implications of the HM2DM model for SUSY collider searches at the Fermilab Tevatron, the CERN LHC, and a 0.5-1.5 TeV linear e^+e^- collider. The sparticle mass spectrum in the HM2DM model qualitatively differs from mSUGRA in several respects: *i*) the low $|\mu|$ parameter implies that charginos and neutralinos should be lighter than in mSUGRA cases with gaugino mass unification and a large $|\mu|$ parameter, so these sparticles should be more accessible to collider searches. In addition, *ii*) the large $|M_2|$ parameter means \widetilde{W}_2 and \widetilde{Z}_4 will be quite heavy and nearly pure wino states, so likely difficult to access at colliders, except perhaps via the (kinematically suppressed) production

and subsequent decays of \tilde{q}_L . Finally, *iii*) the large $|M_2|$ parameter pushes left-sfermion soft terms to higher values, so that the lighter sfermions are dominantly right-sfermions.

In Fig. 12, we show contours of $m_{\tilde{W}_1}$ in the m_0 vs. $m_{1/2}$ plane for $A_0 = 0$, $\tan\beta = 10$ and $\mu > 0$, where at every point M_2 has been dialed up to obtain MHDM with $\Omega_{\tilde{Z}_1} h^2 \sim 0.1$. We see that throughout the plane, $m_{\tilde{W}_1} \sim \frac{1}{2}m_{1/2}$, whereas in mSUGRA, $m_{\tilde{W}_1} \sim \frac{2}{3}m_{1/2}$. This may be of relevance at an e^+e^- collider where the determination of both $m_{\tilde{W}_1}$ and $m_{1/2}$ (via the determination of $m_{\tilde{Z}_1}$) along with M_2 may be possible if $\tilde{W}_1\tilde{W}_2$ production is kinematically accessible.

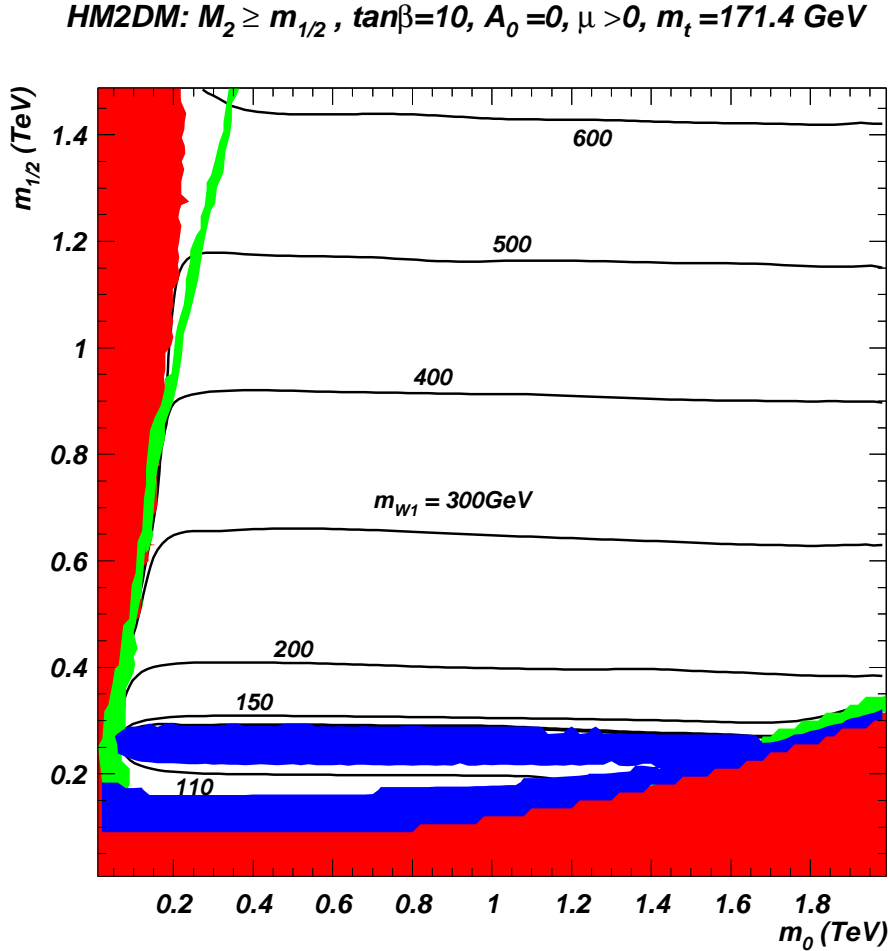


Figure 12: Contours of $m_{\tilde{W}_1}$ in the m_0 vs. $m_{1/2}$ plane for $\tan\beta = 10$, $A_0 = 0$ and $\mu > 0$ where M_2 has been dialed up at every point to yield MHDM where $\Omega_{\tilde{Z}_1} h^2 \sim 0.1$.

In addition, in the HM2DM model, since \tilde{Z}_2 and \tilde{Z}_3 contain large higgsino components while \tilde{Z}_1 is a mixed higgsino-bino state, the mass gaps $m_{\tilde{Z}_3} - m_{\tilde{Z}_1}$ and $m_{\tilde{Z}_2} - m_{\tilde{Z}_1}$ will be expected to be much smaller than in mSUGRA. In mSUGRA, $m_{\tilde{Z}_2} - m_{\tilde{Z}_1} \sim 0.4m_{1/2}$ so that as $m_{1/2}$ grows, the growing $\tilde{Z}_2 - \tilde{Z}_1$ mass gap ultimately allows the $\tilde{Z}_2 \rightarrow \tilde{Z}_1 Z$ or $\tilde{Z}_1 h$ two-body decays to turn on, which dominate the \tilde{Z}_2 branching fraction. The two-body “spoiler” decay modes[72] turn off the leptonic decays $\tilde{Z}_2 \rightarrow \tilde{Z}_1 \ell \bar{\ell}$, which can be the

starting point for sparticle mass reconstruction in gluino and squark cascade decays[73] at hadron colliders. In Fig. 13a), we show the $\tilde{Z}_2 - \tilde{Z}_1$ mass gap in the HM2DM model in the same plane as in Fig. 12. We see that in the case of HM2DM model, the mass gap is everywhere less than M_Z , so that $\tilde{Z}_2 \rightarrow \tilde{Z}_1 \ell \bar{\ell}$ decays will not be shut off by the two-body spoiler modes. Moreover, the mass gap is also almost always larger than ~ 25 GeV, and decreases with increasing $m_{1/2}$ in contrast to the cases of MWDM and DM via BWCA, where the mass gap increases to beyond 100 GeV for the largest values of $m_{1/2}$. This could serve to distinguish HM2DM from other scenarios, something we will return to below. Also, in contrast to mSUGRA as well as the MWDM and BWCA frameworks, in the HM2DM model (and other models with MHDm), we expect that $m_{\tilde{Z}_3} - m_{\tilde{Z}_1}$ cannot be too large because the mass of \tilde{Z}_3 is expected to be not very far above $|\mu|$, as we saw in Fig. 5. In Fig. 13b), we show contours of $m_{\tilde{Z}_3} - m_{\tilde{Z}_1}$. We see that this difference is also everywhere smaller than M_Z , so that the decays $\tilde{Z}_3 \rightarrow \tilde{Z}_1 \ell \bar{\ell}$ and $\tilde{Z}_3 \rightarrow \tilde{Z}_2 \ell \bar{\ell}$ are not shut off by the spoiler modes.

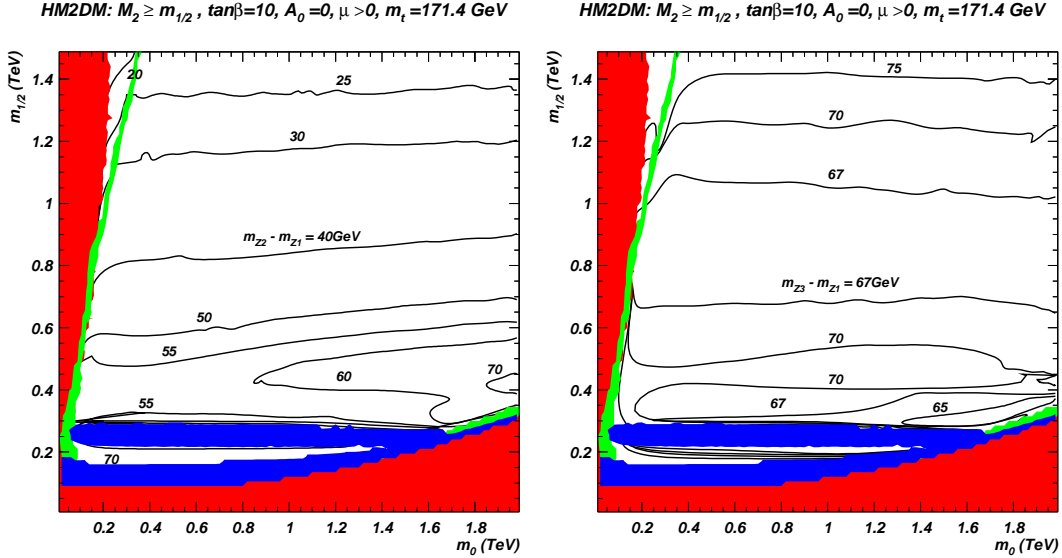


Figure 13: Contours of a) $m_{\tilde{Z}_2} - m_{\tilde{Z}_1}$, and b) $m_{\tilde{Z}_3} - m_{\tilde{Z}_1}$, in the m_0 vs. $m_{1/2}$ plane for $\tan \beta = 10$, $A_0 = 0$ and $\mu > 0$ where M_2 has been dialed up at every point to yield MHDm where $\Omega_{\tilde{Z}_1} h^2 \sim 0.1$.

5.1 Fermilab Tevatron

In the mSUGRA model, since $m_{\tilde{W}_1} > 103.5$ GeV from LEP2 searches, we expect $m_{\tilde{g}} \simeq 3.5 m_{\tilde{W}_1} \gtrsim 350 - 400$ GeV, and this high of sparticle masses generally gives quite low $\tilde{g}\tilde{g}$, $\tilde{q}\tilde{q}$ and $\tilde{g}\tilde{q}$ production cross sections[74]. Gluino and right-squark masses are relatively unchanged in going from mSUGRA to HM2DM, while left-squark masses typically increase. Thus we expect that gluino and squark production rates at the Tevatron will be relatively low, and the signal not easily extracted from data in the HM2DM model.

Another possibility is to look for $p\bar{p} \rightarrow \tilde{W}_1 \tilde{Z}_2 \rightarrow 3\ell + E_T^{\text{miss}}$ [72] in the HM2DM model. The large higgsino components of \tilde{W}_1 and \tilde{Z}_2 imply that $\tilde{W}_1 \tilde{Z}_2$ production via the W^*

will dominantly occur via the isodoublet couplings of the neutralinos to the W . However, this (iso-doublet) $W\widetilde{W}_1\widetilde{Z}_2$ coupling will now be smaller than the corresponding coupling in the mSUGRA framework (where the coupling arises from the iso-triplet components of \widetilde{W}_1 and \widetilde{Z}_2 , and so is very large) so that $\sigma(\widetilde{W}_1\widetilde{Z}_2)$ will be suppressed in HM2DM relative to mSUGRA.

We are thus led to re-examine the rate for trilepton production at the Tevatron in HM2DM model and compare this to the mSUGRA case where the trilepton plus E_T^{miss} signal is regarded as the gold-plated signature. We use the cuts SC2 proposed in Ref. [75] which allow for efficient extraction of the $3\ell + E_T^{\text{miss}}$ signal from various SM backgrounds, the largest of which are $W^*Z^* \rightarrow 3\ell + \nu$ and $W^*\gamma^* \rightarrow 3\ell + \nu$ production. In Fig. 14, we plot the 3ℓ cross section after cuts SC2, fixing $m_0 = 300$ GeV, $A_0 = 0$, $\tan\beta = 10$ and $\mu > 0$ versus $m_{\widetilde{W}_1}$, obtained by varying $m_{1/2}$. Contrary to expectation, we see that the signal is larger in the HM2DM framework than in the mSUGRA case. We have traced this to the fact that the leptonic decay of \widetilde{Z}_2 is very suppressed within the mSUGRA framework, while the corresponding branching fraction is just under $B(Z^0 \rightarrow \ell\bar{\ell}) \simeq 6\%$ as expected for the case of MHDm. In the mSUGRA case, the signal rate is always below the 0.8 fb level. The total background estimated in Ref. [75] is 1.05 fb, which requires a 1.6 fb signal to give a 5σ effect with 10 fb^{-1} of integrated luminosity. The HM2DM curve is enhanced relative to mSUGRA, and reaches a maximum of about 1.4 fb – just below the edge of observability. The dashed region between $m_{\widetilde{W}_1} \sim 117 - 137$ GeV is excluded as can be seen from Fig. 7, while for higher $m_{\widetilde{W}_1}$ values, the signal is always below 0.6 fb, so will be difficult to extract at the Tevatron.

5.2 CERN LHC

At the CERN LHC, gluino and squark pair production is the dominant sparticle production mechanism if sparticle masses are in the TeV range [26]. Gluino and squark cascade decays give rise to events containing multiple hard jets, isolated leptons, E_T^{miss} , and sometimes also isolated photons. The reach of the LHC has been calculated in the mSUGRA model in Refs. [76]. The ultimate reach in the $E_T^{\text{miss}} + \text{jets}$ channel is relatively insensitive to the details of the cascade decays, but depends mostly on the gluino and squark production cross sections, which in turn depends only on their masses.

We have made a rough translation of the LHC reach in the mSUGRA framework to that of the HM2DM model by computing the total production cross section along the 100 fb^{-1} reach contour in the last paper of Ref. [76], and equating it to total production cross sections in the HM2DM m_0 vs. $m_{1/2}$ plane. The result is shown as the dotted contour labelled LHC in Fig. 15. At the small m_0 end, the contour ends up being typically lower in $m_{1/2}$ values by about 150 GeV than the corresponding plots in mSUGRA, with the reduction being smaller for larger values of m_0 . This is because in the HM2DM case, for given m_0 and $m_{1/2}$ values, the various left-squark masses are raised up by a few hundred GeV, causing the corresponding production cross sections to drop. Thus, somewhat lower

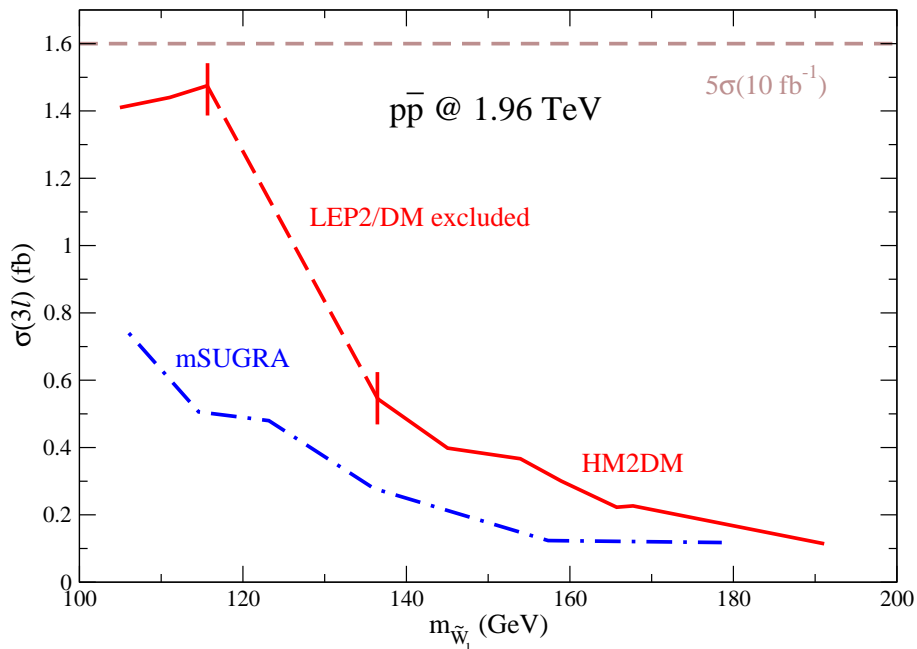


Figure 14: Trilepton signal after cuts SC2 from Ref. [75] versus $m_{\tilde{W}_1}$ along a line of $m_0 = 300$ GeV, variable $m_{1/2}$, adjusted to reproduce the value of $m_{\tilde{W}_1}$, $\tan\beta = 10$, $A_0 = 0$ and $\mu > 0$ where M_2 has been dialed up at every point to yield MHDM where $\Omega_{\tilde{Z}_1} h^2 \sim 0.1$. We also show the corresponding rate from mSUGRA model where $M_2 = m_{1/2}$, and the 5σ discovery level for 10 fb^{-1} of integrated luminosity. The dashed region with $117 \text{ GeV} \lesssim m_{\tilde{W}_1} \lesssim 137 \text{ GeV}$ is excluded in the HM2DM model as can be seen from Fig. 7.

gluino and right-squark masses are needed to obtain the same reach level as mSUGRA within the HM2DM framework. The location of the LHC reach contour in the HM2DM model varies between $m_{1/2} \sim 1260$ GeV at low m_0 and $m_{1/2} \sim 1040$ GeV at $m_0 = 2$ TeV. This corresponds to a reach in terms of gluino mass of $m_{\tilde{g}} \sim 2350 - 2750$ GeV for 100 fb^{-1} of integrated luminosity.

If supersymmetry is discovered at the LHC, reconstruction of SUSY events to measure sparticle masses will be an important item on the experimental agenda. Edges in the distribution of opposite sign, same flavour dilepton masses provide important information on the mass difference $m_{\tilde{Z}_i} - m_{\tilde{Z}_j}$ between those neutralino pairs for which the three body decay $\tilde{Z}_i \rightarrow \tilde{Z}_j \ell \bar{\ell}$ has a significant branching fraction [77]. In the mSUGRA framework, we typically expect an observable edge just for the decays of \tilde{Z}_2 , if its mass is low enough so that the spoiler two body modes are not accessible. However, for the HM2DM model, as for all models with MHDM, both \tilde{Z}_2 and \tilde{Z}_3 are relatively light, so that we may expect more than one mass edge in the dilepton mass spectrum.

To examine this, we simulated 1M LHC SUSY events for the HM2DM1 point in Table 1 using Isajet 7.76, and passed these through a toy detector simulation as described in Ref. [78]. In addition to the various geometric and other acceptance requirements, we

HM2DM: $M_2 \geq m_{1/2}$, $\tan\beta=10$, $A_0=0$, $\mu > 0$, $m_t=171.4$ GeV

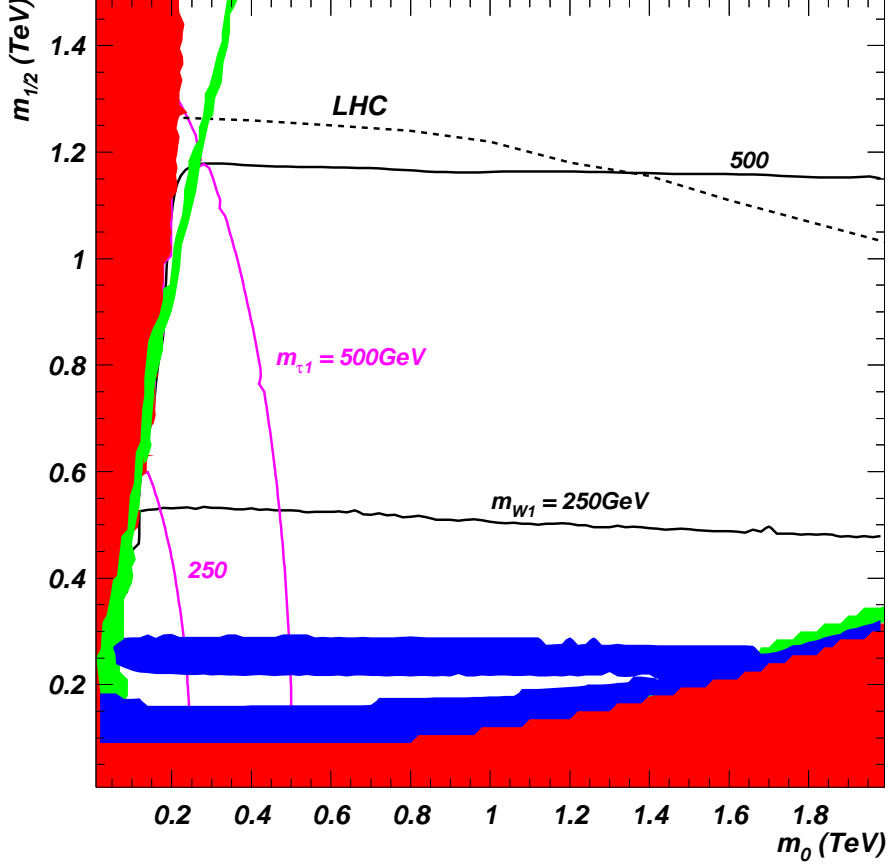


Figure 15: Approximate reach of the CERN LHC (with 100 fb^{-1} of data) and ILC with $\sqrt{s} = 0.5$ and 1 TeV in the HM2DM model, viewed in the m_0 vs. $m_{1/2}$ plane for $\tan\beta = 10$, $A_0 = 0$ and $\mu > 0$ where M_2 has been dialed up at every point to yield MHDm where $\Omega_{\tilde{Z}_1} h^2 \sim 0.1$.

required the following analysis cuts on the signal:

$$E_T^{\text{miss}} > (100 \text{ GeV}, 0.2M_{\text{eff}}),$$

$$n_{\text{jets}} \geq 4,$$

$$E_T(j_1, j_2, j_3, j_4) \geq (150, 150, 80, 50) \text{ GeV},$$

$$S_T \geq 0.2.$$

For the present analysis, we only retain events which include, in addition, a pair of opposite sign (OS) dileptons. The invariant mass distribution for $e^+e^- + \mu^+\mu^-$ pairs in SUSY events is shown by the red-shaded histogram for the signal, and by the line histogram for the SM background, in Fig. 16a). In the signal, these leptons arise from the decays of neutralinos and charginos produced in the SUSY cascade. The mass of dileptons from the three body decay $\tilde{Z}_i \rightarrow \tilde{Z}_j \ell \bar{\ell}$ is kinematically bounded by $m_{\tilde{Z}_i} - m_{\tilde{Z}_j}$, resulting in the

mass edges mentioned above. Lepton pairs where the leptons each come from decays of *different* charginos or neutralinos are uncorrelated in mass, and so are expected to yield a smooth broad continuum. Since these pairs are also uncorrelated in flavour, subtracting the distribution of *unlike-flavour* OS dilepton pairs should (up to statistical fluctuations) leave us with the dilepton mass distribution of dileptons from the same neutralino [79]. This subtracted distribution is shown in Fig. 16b). The following features are worth noting.

1. The red shaded histogram in frame *a*) shows distinct gaps near around 46 GeV and at around 64 GeV, close to the mass edges at 47.6 GeV and 65.4 GeV expected from the leptonic decays of \tilde{Z}_2 and \tilde{Z}_3 to the LSP, respectively. There is no corresponding gap near $m_{\tilde{Z}_3} - m_{\tilde{Z}_2}$ indicating that the branching fraction $B(\tilde{Z}_3 \rightarrow \tilde{Z}_2 \ell \bar{\ell})$ is very small (0.2% per lepton flavour in the present case).
2. There is a distinct peak at M_Z showing that Z bosons are being produced in SUSY cascades. This is a strong indication (even if not evidence) of the production of \tilde{W}_2 and/or \tilde{Z}_4 , since the only other source of Z 's would be the decays $\tilde{t}_2 \rightarrow \tilde{t}_1 Z$, $\tilde{b}_2 \rightarrow \tilde{b}_1 Z$ or $A \rightarrow hZ$, all of which are likely to have very small cross sections in many models.
3. The subtracted distribution in frame *b*) also shows these edges even though the location of the $m_{\tilde{Z}_2} - m_{\tilde{Z}_1}$ edge seems somewhat smeared out by an upward fluctuation in the opposite flavour OS dilepton distribution in the mass bin just below 60 GeV, resulting instead in a shoulder around the expected value.
4. The large levels of the background in some bins are caused by a handful of QCD events passing our cuts. Because of the large QCD cross section, we need to simulate a much larger sample of QCD events than we were able to in order to further reduce these fluctuations.⁸ We expect though that the QCD background to the SUSY signal will be under control at the LHC.
5. Finally, we observe that in both frames the shape of the dilepton distribution in the region below the first edge, and in between the two edges is very different. Specifically, the $m_{\tilde{Z}_3} - m_{\tilde{Z}_1}$ mass edge is much sharper than the $m_{\tilde{Z}_2} - m_{\tilde{Z}_1}$ edge. This is due to the difference in shapes of the mass distributions of dileptons from the decays of \tilde{Z}_2 and \tilde{Z}_3 . As pointed out by Kitano and Nomura in Ref. [80], this shape depends on the relative sign of the mass eigenvalue of the parent and daughter neutralino. If this relative sign is positive, we get a sharp mass edge as is the case for the $m_{\tilde{Z}_3} - m_{\tilde{Z}_1}$ edge in the figure. Since \tilde{Z}_2 and \tilde{Z}_3 are dominantly the higgsino states, not surprisingly they then have opposite signs for the eigenvalues, causing the distribution of dileptons from $\tilde{Z}_2 \rightarrow \ell \bar{\ell} \tilde{Z}_1$ to peak at lower values of $m(\ell^+ \ell^-)$ so that the $m_{\tilde{Z}_2} - m_{\tilde{Z}_1}$ edge is much more diffuse. The shape of the dilepton distribution thus provides important information about the composition of neutralinos.

⁸It is not clear that such a computer-intensive simulation of the tail of this detector-dependent background would be particularly meaningful, especially in view of our toy calorimeter simulation.

5.3 Linear e^+e^- collider

In assessing the role of the ILC for a discovery of SUSY within the HM2DM framework, we first note that, for a fixed value of m_0 and $m_{1/2}$, the value of $m_{\widetilde{W}_1}$ is lowered with respect to mSUGRA. This is because in the HM2DM model, $|\mu|$ is lowered to below $\sim 2M_1$, which is approximately the \widetilde{W}_1 mass in models with unified gaugino masses. This increases the reach of ILC in m_0 vs. $m_{1/2}$ space while at the same time the LHC reach is slightly diminished due to the increased left-squark masses. We show in Fig. 15 the approximate ILC reach for a $\sqrt{s} = 0.5$ and 1 TeV machines by delineating the mass contours where $m_{\widetilde{W}_1}$ and $m_{\widetilde{\tau}_1} = 250$ and 500 GeV (some additional region may be accessible beyond this via $\widetilde{Z}_1\widetilde{Z}_2$ production [81]). The bulk of the ILC reach for a $\sqrt{s} = 0.5$ TeV machine reaches to the $m_{1/2} \sim 500$ GeV level, corresponding to a gluino mass of ~ 1150 GeV. A $\sqrt{s} = 1$ TeV ILC has a reach extending to $m_{1/2} \sim 1150$ GeV, corresponding to a value of $m_{\widetilde{g}} \sim 2600$ GeV. The enhanced reach of ILC coupled to decreased reach of LHC in terms of $m_{1/2}$ means that a 1 TeV ILC has a comparable reach to the LHC.

Within the HM2DM model, we have $M_1 \lesssim |\mu| \ll M_2$ at the weak scale. Thus if gluinos (remember that $m_{\widetilde{g}} \sim 6M_1$) are accessible at the LHC, it is reasonable to expect that \widetilde{W}_1 as well as \widetilde{Z}_1 , \widetilde{Z}_2 and \widetilde{Z}_3 will be accessible at a TeV linear collider. The HM2DM framework will be readily distinguishable from the mSUGRA model if chargino pair production is kinematically accessible. Since the chargino is mainly a wino in mSUGRA, and a higgsino in the HM2DM model, the total chargino pair production cross section (for a given value of $m_{\widetilde{W}_1}$) as well as its dependence on the polarization of the electron beam is very different. In the mSUGRA case, the expected cross section is significantly larger than in the HM2DM model, and further, drops to very low values as the electron beam is taken to be increasingly right-handed, while this same dependence is comparably milder for the higgsino-like \widetilde{W}_1 . This may be corroborated by studying the polarization-dependence of

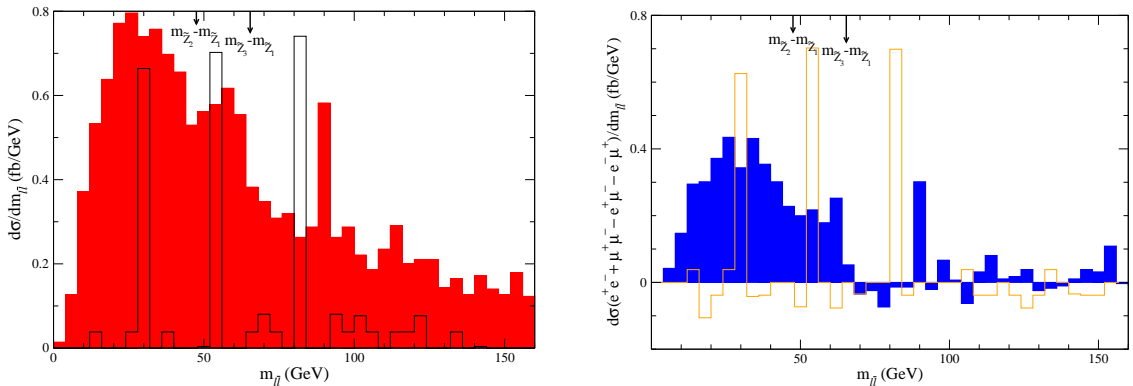


Figure 16: a) Distribution of the invariant mass of same flavor/opposite sign dilepton pairs in SUSY events at the CERN LHC (red histogram) after the cuts discussed in the text, along with the expectation for the corresponding SM background (open histogram). b) The difference between this distribution and the corresponding one with opposite flavour/opposite sign dileptons in SUSY events (blue histogram) along with the SM background (open histogram). The signal distributions are calculated for the HM2DM1 case in Table 1.

neutralino pair production. Within mSUGRA, the polarization dependence of the wino-like \tilde{Z}_2 pairs is similar to that of chargino pair production, while the higgsino-like \tilde{Z}_3 and \tilde{Z}_4 are typically heavy. For the MHDM case realized in the HM2DM framework, on the other hand, \tilde{Z}_1 , \tilde{Z}_2 and \tilde{Z}_3 are light and mixed, so that not only are several $\tilde{Z}_i\tilde{Z}_j$ pairs accessible, the polarization dependence and size of the cross sections is very different.

This is illustrated in Fig. 17, where we show various -ino pair production cross sections accessible to a $\sqrt{s} = 0.5$ TeV ILC versus beam polarization $P_L(e^-)$ in the case of *a*) the mSUGRA model case and *b*) for the HM2DM1 case in Table 1. In frame *a*), we see that only $\tilde{W}_1^+\tilde{W}_1^-$, $\tilde{Z}_1\tilde{Z}_2$ and $\tilde{Z}_2\tilde{Z}_2$ are accessible to a 0.5 TeV ILC, and that their cross sections precipitously drop from readily observable values of tens or hundreds of femtobarns to below 1 fb, as the electron beam polarization becomes increasingly right-handed. In the HM2DM case shown in frame *b*), we see that as anticipated many more -ino pair production reactions are accessible, with vastly differing cross sections. The production of one chargino and three neutralino states should be unambiguous. The relative size of the various neutralino cross sections will be parameter-dependent: in the present case the small size of $\sigma(\tilde{Z}_2\tilde{Z}_2)$ is a reflection of the fact that the magnitudes of the \tilde{h}_u and \tilde{h}_d components of \tilde{Z}_2 are nearly equal. The polarization dependence of the (higgsino-like) neutralino production cross sections is also different from frame *a*). A detailed study of the -ino production reactions should allow the determination of M_1 and μ [82].

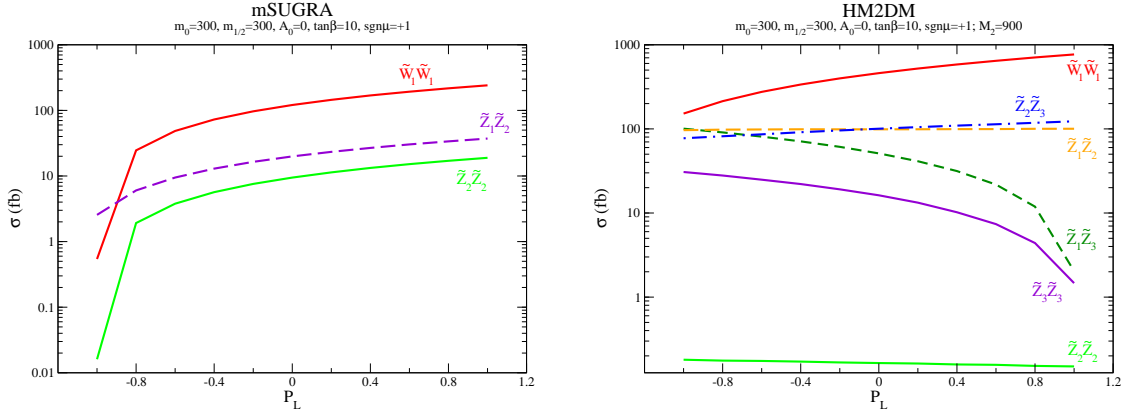


Figure 17: Cross section for $\tilde{W}_1^+\tilde{W}_1^-$ and $\tilde{Z}_i\tilde{Z}_j$ production at a $\sqrt{s} = 0.5$ TeV linear collider versus beam polarization parameter $P_L(e^-)$ for $m_0 = 300$ GeV, $m_{1/2} = 300$ GeV, $A_0 = 0$, $\tan\beta = 10$ and $\mu > 0$ in the *a*) mSUGRA model and *b*) HM2DM model with $M_2 = 900$ GeV.

Another feature of the HM2DM model is that, since M_2 is large and feeds into sfermion masses via the RG running from a universal scalar mass, we expect the lightest sfermions to be dominantly right-type, and the heaviest are dominantly left-type. Within mSUGRA, the sfermions of the first two generations are approximately degenerate, while for the third generation only the τ -sleptons and top squarks are dominantly right-handed, while large top quark Yukawa effects make \tilde{b}_1 mostly the left-type, as illustrated in Fig. 6. We illustrate the beam polarization dependence of third generation sfermion pair production cross sections at a hypothetical $\sqrt{s} = 1.5$ TeV ILC in Fig. 18 for *a*) the mSUGRA model point in Table 1 and *b*) the case HM2DM2 case in Table 1. It is clear in the mSUGRA

model from the polarization dependence that in fact $\tilde{\tau}_1$ is dominantly right-type, \tilde{b}_1 is dominantly left-type and \tilde{t}_1 is mixed left-right. While the polarization dependence for stau and stop pair production is qualitatively similar in the two models, that for b -squark pair production is markedly different, providing a clear signature for the qualitatively different value of θ_b in the HM2DM model.

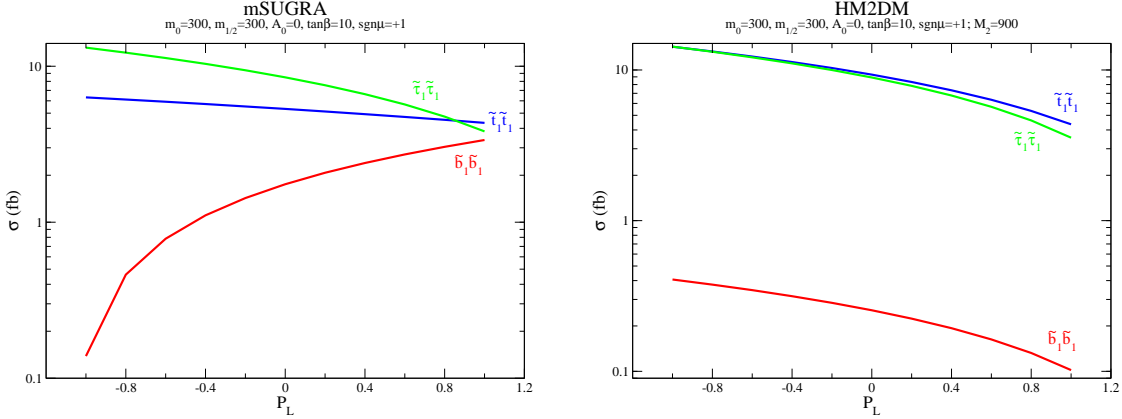


Figure 18: Cross section for $\tilde{t}_1\tilde{t}_1$, $\tilde{b}_1\tilde{b}_1$ and $\tilde{\tau}_1^+\tilde{\tau}_1^-$ production at a $\sqrt{s} = 1500$ GeV linear collider versus beam polarization parameter $P_L(e^-)$ for $m_0 = 300$ GeV, $m_{1/2} = 300$ GeV, $A_0 = 0$, $\tan\beta = 10$ and $\mu > 0$ in the a) mSUGRA model and b) HM2DM model case with $M_2 = 900$ GeV in Table 1.

6. Summary and concluding remarks

While the recently measured value of the CDM relic density can be accommodated within the paradigm mSUGRA framework, much of the allowed region lies at the edge of the parameter space as exemplified by many studies in the $m_0 - m_{1/2}$ plane. There are, however, several one-parameter extensions of the mSUGRA model where it is possible to get the observed value of $\Omega_{\text{CDM}}h^2$ all over this plane for essentially all values of $\tan\beta$ and A_0 . These extensions involve either the adjustment of the mass spectrum (so that the neutralino annihilation rate is enhanced via an s -channel A/H resonance or via co-annihilation with a charged sparticle) or the adjustment of the neutralino composition (to obtain either MWDM or MHDM). MHDM requires a reduced value of μ^2 , and several models that lead to small $|\mu|$ have been proposed. In this paper, we have pointed out a new mechanism for obtaining the observed relic density: non-universal boundary conditions with a large GUT scale value of the $SU(2)$ gaugino mass parameter $|M_2|$ can lead to MHDM. We have also studied the broad phenomenological implications of this scenario.

Common to all scenarios with MHDM, our scenario has an -ino spectrum where the lightest neutralino is a mixed bino-higgsino state, the lighter chargino and the next two heavier neutralinos have large higgsino content, while the heaviest chargino and neutralino are dominantly wino-like with a mass $|M_2|$ considerably larger than the other -ino masses. In the HM2DM model, $|M_2|$ is raised even further and the wino states become very heavy and would likely only be produced at the LHC via cascade decays of \tilde{q}_L . The feature that distinguishes the HM2DM model from other models with MHDM is that *weak interaction*

effects make the left-sfermions significantly heavier than their right-siblings. This effect leads to a qualitative change in the intrageneration mixing pattern of b -squarks: in the HM2DM model, \tilde{b}_1 is dominantly right-handed, while in most models (with universal mass parameters for \tilde{b}_L and \tilde{b}_R) top-quark Yukawa coupling effects make \tilde{b}_1 mostly left-handed.

As in all models with MHD, direct search experiments provide a promising avenue once they reach a sensitivity to probe neutralino-nucleon scattering cross sections $\lesssim 10^{-8}$ pb. With an order of magnitude increase in sensitivity (projected at superCDMS or at $\gtrsim 100$ kg noble liquid detectors), there should be an observable signal over most of the parameter space, while ton-sized noble element detectors should be able to probe the entire parameter space. Our conclusions for indirect searches are less definitive since, except for IceCube type detectors, the signals depend on assumptions of the distribution of the DM in our galactic halo. While IceCube may well be sensitive to the signal, the best prospects for anti-particle detection appear to come from the search for anti-deuterons. For the case that we examined, the Pamela satellite that is currently gathering data may just be sensitive enough to the signal from anti-protons for a favourable halo profile, but less so for the positron signal. The dependence of the gamma ray signal from our galactic center on the halo profile is too large to draw strong conclusions about the observability in GLAST, but perhaps a signal in anti-particle searches may make the situation clearer.

We have discussed collider signals in Sec. 5. Prospect for a discovery at the Tevatron are not encouraging within this scenario. While the reach of the LHC is slightly degraded relative to its reach in the mSUGRA model, experiments at the LHC should be sensitive to gluino masses as large as 2750 GeV (2350 GeV) for a small (moderate) value of m_0 , assuming an integrated luminosity of 100 fb. The TeV linear collider should be sensitive to a discovery in a parameter space region very similar to the LHC. Searches in the multi-jet plus opposite sign dileptons plus E_T^{miss} channel will be especially interesting as the dilepton mass distribution for same flavour lepton pairs may not only allow the construction of more than one mass edge (strongly suggestive of MHD), but may also, via its shape, provide indirect evidence for a higgsino-like \tilde{Z}_2/\tilde{Z}_3 .

It should be possible, at least in principle, to distinguish the HM2DM model discussed here from other scenarios that also lead to agreement with the observed relic density. Within a supersymmetric interpretation of an observed signal at the LHC, the observation of more than one dilepton mass edge would point to the existence of \tilde{Z}_2 and \tilde{Z}_3 with a relatively small mass splitting ($\leq M_Z$) between \tilde{Z}_1 and these neutralinos. In turn, this would point to a small value of $|\mu|$.⁹ If we further *assume* that the CDM density is *saturated* by the LSP, we know that \tilde{Z}_1 cannot be the higgsino. Recall that for $M_1 \ll |\mu| \ll M_2$, $m_{\tilde{Z}_1} \simeq M_1$ while $m_{\tilde{Z}_2}$ and $m_{\tilde{Z}_3}$ would be on either side of $|\mu|$ so that the value of $|\mu| - m_{\tilde{Z}_1}$ must lie between the $m_{\tilde{Z}_3} - m_{\tilde{Z}_1}$ and $m_{\tilde{Z}_2} - m_{\tilde{Z}_1}$ mass edges. We note, however, that while the second inequality always holds within the HM2DM model, $|\mu|$ may not always be that much larger than M_1 as, for instance, in the HM2DM1 case. The mass edges nevertheless serve as a semi-quantitative indicator of $|\mu|$ relative to $m_{\tilde{Z}_1}$, and so may provide

⁹It is, of course, logically possible that M_2 is just a bit smaller than $|\mu|$ so that all four neutralinos are strongly mixed and accessible, but with $m_{\tilde{Z}_4} - m_{\tilde{Z}_1} > M_Z$. In this case it would not be unreasonable to expect additional mass edges from decays of the heavier neutralinos to \tilde{Z}_2 , or perhaps even to \tilde{Z}_3 .

corroborative evidence for consistency with the MHDM hypothesis. A striking confirmation of the MHDM hypothesis could come from the observation of a large cross section in direct DM search experiments. While the dilepton mass edges may serve to separate out the MHDM scenarios from those with MWDM or BWCA, they do not provide evidence for the HM2DM framework, since this would likely require a complete reconstruction of the \tilde{W} -ino sector with a precision difficult at the LHC. Aside from a determination of M_2 via that of $m_{\tilde{W}_2}$ (or $m_{\tilde{Z}_4}$), the smoking gun for the HM2DM framework would be observing a wino-like \tilde{W}_2/\tilde{Z}_4 and/or a large splitting between the left and right sfermions, or determining that the lighter b -squark state is mainly \tilde{b}_R . None of these appear straightforward at the LHC. It is unlikely the heavier slepton or chargino will be accessible at the LHC in this scenario, and squark mass splittings and mixing angles are difficult to measure there. A high energy electron-positron collider offers the best prospects for these measurements, assuming, of course, that these sparticles are kinematically accessible.

Acknowledgments

This research was supported in part by grants from the U.S. Department of Energy. HB would like to thank the CERN theory group and LHC/cosmology visitor program for hospitality while this work was completed.

References

- [1] D. N. Spergel *et al.* (WMAP Collaboration), [astro-ph/0603449](#) (2006).
- [2] H. Goldberg, *Phys. Rev. Lett.* **50** (1419) 1983; J. Ellis, J. Hagelin, D. Nanopoulos and M. Srednicki, *Phys. Lett.* **B127**, 233 (1983); J. Ellis, J. Hagelin, D. Nanopoulos, K. Olive and M. Srednicki, *Nucl. Phys.* **B238**, 453 (1984).
- [3] For recent reviews, see *e.g.* C. Jungman, M. Kamionkowski and K. Griest, *Phys. Rept.* **267** (195) 1996; A. Lahanas, N. Mavromatos and D. Nanopoulos, *Int. J. Mod. Phys.* **D 12** (2003) 1529; M. Drees, [hep-ph/0410113](#); K. Olive, “Tasi Lectures on Astroparticle Physics”, [astro-ph/0503065](#).
- [4] G. Gelmini and P. Gondolo, *Phys. Rev.* **D 74** (2006) 023510.
- [5] J. Ellis, K. Olive, Y. Santoso and V. Spanos, *Phys. Lett.* **B 565** (2003) 176; H. Baer and C. Balazs, *JCAP* **0305** (2003) 006; U. Chattopadhyay, A. Corsetti and P. Nath, *Phys. Rev.* **D 68** (2003) 035005; A. Lahanas and D. V. Nanopoulos, *Phys. Lett.* **B 568** (2003) 55; A. Djouadi, M. Drees and J. Kneur, [hep-ph/0602001](#); for a review, see A. Lahanas, N. Mavromatos and D. Nanopoulos, Ref. [3].
- [6] A. Chamseddine, R. Arnowitt and P. Nath, *Phys. Rev. Lett.* **49** (1982) 970; R. Barbieri, S. Ferrara and C. Savoy, *Phys. Lett.* **B 119** (1982) 343; N. Ohta, *Prog. Theor. Phys.* **70** (1983) 542; L. J. Hall, J. Lykken and S. Weinberg, *Phys. Rev.* **D 27** (1983) 2359; for reviews, see H. P. Nilles, *Phys. Rep.* **110** (1984) 1, and P. Nath, [hep-ph/0307123](#).
- [7] H. Baer and M. Brhlik, *Phys. Rev.* **D 53** (1996) 597; V. Barger and C. Kao, *Phys. Rev.* **D 57** (1998) 3131.

- [8] J. Ellis, T. Falk and K. Olive, *Phys. Lett.* **B 444** (1998) 367; J. Ellis, T. Falk, K. Olive and M. Srednicki, *Astropart. Phys.* **13** (2000) 181; M.E. Gómez, G. Lazarides and C. Pallis, *Phys. Rev.* **D 61** (2000) 123512 and *Phys. Lett.* **B 487** (2000) 313; A. Lahanas, D. V. Nanopoulos and V. Spanos, *Phys. Rev.* **D 62** (2000) 023515; R. Arnowitt, B. Dutta and Y. Santoso, *Nucl. Phys.* **B 606** (2001) 59; see also Ref. [31]
- [9] C. Böhm, A. Djouadi and M. Drees, *Phys. Rev.* **D 30** (2000) 035012; J. R. Ellis, K. A. Olive and Y. Santoso, *Astropart. Phys.* **18** (2003) 395; J. Edsjö, *et al.*, *JCAP* **0304** (2003) 001
- [10] K. L. Chan, U. Chattopadhyay and P. Nath, *Phys. Rev.* **D 58** (1998) 096004. J. Feng, K. Matchev and T. Moroi, *Phys. Rev. Lett.* **84** (2000) 2322 and *Phys. Rev.* **D 61** (2000) 075005; see also H. Baer, C. H. Chen, F. Paige and X. Tata, *Phys. Rev.* **D 52** (1995) 2746 and *Phys. Rev.* **D 53** (1996) 6241; H. Baer, C. H. Chen, M. Drees, F. Paige and X. Tata, *Phys. Rev.* **D 59** (1999) 055014; for a model-independent approach, see H. Baer, T. Krupovnickas, S. Profumo and P. Ullio, *J. High Energy Phys.* **0510** (2005) 020.
- [11] M. Drees and M. Nojiri, *Phys. Rev.* **D 47** (1993) 376; H. Baer and M. Brhlik, *Phys. Rev.* **D 57** (1998) 567; H. Baer, M. Brhlik, M. Diaz, J. Ferrandis, P. Mercadante, P. Quintana and X. Tata, *Phys. Rev.* **D 63** (2001) 015007; J. Ellis, T. Falk, G. Ganis, K. Olive and M. Srednicki, *Phys. Lett.* **B 510** (2001) 236; L. Roszkowski, R. Ruiz de Austri and T. Nihei, *J. High Energy Phys.* **0108** (024) 2001; A. Djouadi, M. Drees and J. L. Kneur, *J. High Energy Phys.* **0108** (2001) 055; A. Lahanas and V. Spanos, *Eur. Phys. J.* **C 23** (2002) 185.
- [12] R. Arnowitt and P. Nath, *Phys. Rev. Lett.* **70** (1993) 3696; H. Baer and M. Brhlik, Ref. [7]; A. Djouadi, M. Drees and J. Kneur, *Phys. Lett.* **B 624** (2005) 60.
- [13] H. Baer, A. Belyaev, T. Krupovnickas and A. Mustafayev, *J. High Energy Phys.* **0406** (2004) 044.
- [14] V. Berezhinski *et al.* *Astropart. Phys.* **5** (1996) 333; P. Nath and R. Arnowitt, *Phys. Rev.* **D 56** (1997) 2820; A. Bottino, F. Donato, N. Fornengo and S. Scopel, *Phys. Rev.* **D 59** (1999) 095004 and *Phys. Rev.* **D 63** (2001) 125003; J. Ellis, K. Olive and Y. Santoso, *Phys. Lett.* **B 539** (2002) 107; J. Ellis, T. Falk, K. Olive and Y. Santoso, *Nucl. Phys.* **B 652** (2003) 259; M. Drees, hep-ph/0410113; H. Baer, A. Mustafayev, S. Profumo, A. Belyaev and X. Tata, *Phys. Rev.* **D 71** (2005) 095008 and *J. High Energy Phys.* **0507** (2005) 065.
- [15] M. Drees *Phys. Lett.* **B 158** (1985) 409; G. Anderson *et al.* in *New Directions in High Energy Physics, Proc. Snowmass 96 V2*, p 669; G. Anderson, H. Baer, C-H. Chen and X. Tata, *Phys. Rev.* **D 61** (2000) 095005.
- [16] A. Birkedal-Hansen and B. Nelson, *Phys. Rev.* **D 64** (2001) 015008 and *Phys. Rev.* **D 67** (2003) 095006; H. Baer, A. Mustafayev, E. K. Park and S. Profumo, *J. High Energy Phys.* **0507** (2005) 046.
- [17] D. Auto, H. Baer, A. Belyaev and T. Krupovnickas, *J. High Energy Phys.* **0410** (2004) 066.
- [18] H. Baer, T. Krupovnickas, A. Mustafayev, E. K. Park, S. Profumo and X. Tata, *J. High Energy Phys.* **0512** (2005) 011.
- [19] G. Belanger, F. Boudjema, A. Cottrant, A. Pukhov and A. Semenov, *Nucl. Phys.* **B 706** (2005) 411; Y. Mambrini and E. Nezri, *Eur. Phys. J.* **C 50** (2007) 949.
- [20] H. Baer, A. Mustafayev, E. K. Park, S. Profumo and X. Tata, *J. High Energy Phys.* **0604** (2006) 041; H. Baer, A. Mustafayev, S. Profumo and X. Tata, *Phys. Rev.* **D 75** (2007) 035004.

- [21] N. Arkani-Hamed, A. Delgado and G. F. Giudice, [hep-ph/0601041](#) (2006).
- [22] H. Baer, A. Mustafayev, E. K. Park and X. Tata, *JCAP* **0701** (2007) 017.
- [23] K. Choi, K-S. Jeong and K. Okumura, *J. High Energy Phys.* **0509** (2005) 039; M. Endo, M. Yamaguchi and K. Yoshioka, *Phys. Rev. D* **72** (2005) 015004; A. Falkowski, O. Lebedev and Y. Mambrini, *J. High Energy Phys.* **0511** (2005) 034; H. Baer, E. K. Park, X. Tata and T. Wang, *J. High Energy Phys.* **0608** (2006) 041, *Phys. Lett. B* **641** (2006) 447 and [hep-ph/0703024](#); K. Choi, K. Y. Lee, Y. Shimizu, Y. G. Kim and K. Okumura, *JCAP* **0612** (2006) 017.
- [24] S. Martin, *Phys. Rev. D* **75** (2007) 115005.
- [25] H. Baer, A. Box, E. K. Park and X. Tata, *J. High Energy Phys.* **0708** (2007) 060; S. Martin, [arXiv:0707.2812](#) (2007) [hep-ph].
- [26] H. Baer and X. Tata, *Weak Scale Supersymmetry: From Superfields to Scattering Events*, (Cambridge University Press, 2006).
- [27] M. Drees, R. Godbole and P. Roy, *Theory and Phenomenology of Sparticles*, (World Scientific, 2004).
- [28] L. E. Ibanez and G. G. Ross, *Phys. Lett. B* **110** (1982) 215; L. Ibanez, *Phys. Lett. B* **118** (1982) 73; J. Ellis, D. V. Nanopoulos and K. Tamvakis, *Phys. Lett. B* **121** (1983) 123; L. Alvarez-Gaume, J. Polchinski and M. B. Wise, *Nucl. Phys. B* **221** (1983) 495.
- [29] CDF and D0 collaborations, [hep-ph/0703034](#) (2007).
- [30] ISAJET, by H. Baer, F. Paige, S. Protopopescu and X. Tata, [hep-ph/0312045](#); see also H. Baer, J. Ferrandis, S. Kraml and W. Porod, *Phys. Rev. D* **73** (2006) 015010.
- [31] IsaRED, by H. Baer, C. Balazs and A. Belyaev, *J. High Energy Phys.* **0203** (2002) 042.
- [32] E. Barberio *et al.* (Heavy Flavor Averaging Group), [hep-ex/0603003](#).
- [33] J. Ellis, K. Olive and Y. Santoso, *Phys. Lett. B* **539** (2002) 107; J. Ellis, T. Falk, K. Olive and Y. Santoso, *Nucl. Phys. B* **652** (2003) 259.
- [34] H. Baer, A. Belyaev, T. Krupovnickas and J. O’Farrill, *JCAP* **0404** (2004) 005.
- [35] W. M. Yao *et al.* (Particle Data Group), *J. Phys. G* **33** (2006) 1. For the recent results from the E821 collaboration, see G. W. Bennett *et al.* *Phys. Rev. D* **73** (2006) 072003, and references cited therein.
- [36] M. Davier, [arXiv:hep-ph/0701163](#) (2007); see also, K. Hagiwara, A. D. Martin, D. Nomura and T. Teubner, *Phys. Lett. B* **649** (2007) 173.
- [37] See *e.g.* H. Baer and M. Brhlik, *Phys. Rev. D* **55** (1997) 3201 and H. Baer, M. Brhlik, D. Castaño and X. Tata, *Phys. Rev. D* **58** (1998) 015007, and references cited therein.
- [38] K. Chetyrkin, M. Misiak and M. Munz, *Phys. Lett. B* **400** (1997) 206 and erratum-ibid, *Phys. Lett. B* **425** (1998) 414; A. Buras *et al.*, *Phys. Lett. B* **414** (1997) 157 and erratum-ibid, *Phys. Lett. B* **434** (1998) 459; A. Kagan and M. Neubert, *Eur. Phys. J. C* **7** (1999) 5.
- [39] For a review, see *e.g.* G. Eigen, R. Gaitskell, G. Kribs and K. Matchev, [hep-ph/0112312](#); see also D. Hooper and L. T. Wang, *Phys. Rev. D* **69** (2004) 035001; W. de Boer, M. Herold, C. Sander and V. Zhukov, [hep-ph/0309029](#).
- [40] H. Baer, C. Balazs, A. Belyaev and J. O’Farrill, *JCAP* **0309**, 2003 (007)

- [41] P. Gondolo, J. Edsjo, P. Ullio, L. Bergstrom, M. Schelke and E. A. Baltz, [astro-ph/0211238](#).
- [42] J. F. Navarro et al., *Mon. Not. Roy. Astron. Soc.* **349** (2004) 1039, [astro-ph/0311231](#); the adiabatic contraction of the halo follows Blumental et al., *Astrophys. J.* **301** (1986) 27. For the halo parameter choices see also Ref. [45].
- [43] A. Burkert, *Astrophys. J.* **447** (1995) L25; P. Salucci and A. Burkert, *Astrophys. J.* **537** (2000) L9.
- [44] H. Baer and J. O’Farrill, *JCAP* **0403** (2004) 012.
- [45] S. Profumo and P. Ullio, *JCAP* **0407** (2004) 006.
- [46] For a recent analysis, see Ref. [40]; a subset of earlier work includes M. Goodman and E. Witten, *Phys. Rev. D* **31** (1985) 3059; K. Griest, *Phys. Rev. Lett.* **61** (1988) 666 and *Phys. Rev. D* **38** (1988) 2357 [Erratum-ibid. *D* **39**, 3802 (1989)]; M. Drees and M. Nojiri, *Phys. Rev. D* **47** (1993) 4226 and *Phys. Rev. D* **48** (1993) 3483; V. A. Bednyakov, H. V. Klapdor-Kleingrothaus and S. Kovalenko, *Phys. Rev. D* **50** (1994) 7128; P. Nath and R. Arnowitt, *Phys. Rev. Lett.* **74** (1995) 4592; L. Bergstrom and P. Gondolo, *Astropart. Phys.* **5** (1996) 263; H. Baer and M. Brhlik, *Phys. Rev. D* **57** (1998) 567; J. Ellis, A. Ferstl and K. Olive, *Phys. Lett. B* **481** (2000) 304 and *Phys. Rev. D* **63** (2001) 065016; E. Accomando, R. Arnowitt, B. Dutta and Y. Santoso, *Nucl. Phys. B* **585** (2000) 124; A. Bottino, F. Donato, N. Fornengo and S. Scopel, *Phys. Rev. D* **63** (2001) 125003; M. E. Gomez and J. D. Vergados, *Phys. Lett. B* **512** (2001) 252; A. B. Lahanas, D. V. Nanopoulos and V. C. Spanos, *Phys. Lett. B* **518** (2001) 94; A. Corsetti and P. Nath, *Phys. Rev. D* **64** (2001) 115009; E. A. Baltz and P. Gondolo, *Phys. Rev. Lett.* **86** (2001) 5004; M. Drees, Y. G. Kim, T. Kobayashi and M. M. Nojiri, *Phys. Rev. D* **63** (2001) 115009; see also J. Feng, K. Matchev and F. Wilczek, *Phys. Lett. B* **482** (2000) 388 and *Phys. Rev. D* **63** (2001) 045024; R. Ellis, A. Ferstl, K. A. Olive and Y. Santoso, *Phys. Rev. D* **67** (2003) 123502; J. R. Ellis, K. A. Olive, Y. Santoso and V. C. Spanos, *Phys. Rev. D* **69** (2004) 015005; see C. Munoz, [hep-ph/0309346](#) for a recent review.
- [47] J. Angle *et al.* (XENON collaboration) [arXiv:0706.0039](#) (2007) [astro-ph].
- [48] D. S. Akerib *et al.* (CDMS Collaboration), [astro-ph/0405033](#) (2004).
- [49] A. Benoit *et al.* (Edelweiss Collaboration), *Phys. Lett. B* **545** (2002) 43.
- [50] M. Bravin *et al.* (CRESST Collaboration), *Astrophys. J.* **12** (1999) 107.
- [51] N. Spooner *et al.* (Zeplin-1 Collaboration), in *Proc. of the APS/DPF/DPB Summer Study on the Future of Particle Physics (Snowmass 2001)* ed. N. Graf, eConf **C010630**, E601 (2001).
- [52] J. R. Ellis, K. A. Olive, Y. Santoso and V. C. Spanos, *Phys. Rev. D* **71** (2005) 095007.
- [53] Y. Suzuki *et al.* (Xenon Collaboration), [hep-ph/0008296](#).
- [54] See talk by C. Rubbia at 6th UCLA Symposium on *Sources and Detection of Dark Matter and Dark Energy in the Universe*, Marina del Ray, CA, February (2004).
- [55] J. A. Nikkel, W. H. Lippincott and D. N. McKinsey, *Int. J. Mod. Phys. A* **20** (2005) 3113.
- [56] J. Silk, K. Olive and M. Srednicki, *Phys. Rev. Lett.* **55** (1985) 257; K. Freese, *Phys. Lett. B* **167** (1986) 295; L. Krauss, M. Srednicki and F. Wilczek, *Phys. Rev. D* **33** (1986) 2079; V. Berezhinsky, A. Bottino, J. R. Ellis, N. Fornengo, G. Mignola and S. Scopel, *Astropart. Phys.* **5** (1996) 333; L. Bergstrom, J. Edsjo and P. Gondolo, *Phys. Rev. D* **55** (1997) 1765 and *Phys. Rev. D* **58** (1998) 103519; A. Bottino, F. Donato, N. Fornengo and S. Scopel,

- Astropart. Phys.* **10** (1999) 203; A. Corsetti and P. Nath, *Int. J. Mod. Phys. A* **15** (2000) 905; V. Barger, F. Halzen, D. Hooper and C. Kao, *Phys. Rev. D* **65** (2002) 075022; V. Bertin, E. Nezri and J. Orloff, *Eur. Phys. J. C* **26** (2002) 111 and *J. High Energy Phys.* **0302** (2003) 046.
- [57] E. Carmona *et al.*, (Antares Collaboration), *Nucl. Phys.* **95** (*Proc. Suppl.*) (2001) 161.
- [58] J. Ahrens *et al.*, (IceCube Collaboration), *Nucl. Phys.* **118** (*Proc. Suppl.*) (2003) 388; F. Halzen, [astro-ph/0311004](#); F. Halzen and D. Hooper, *JCAP* **0401** (2004) 002.
- [59] F. Stecker, *Phys. Lett. B* **201** (1988) 529; F. W. Stecker and A. J. Tylka, *Astrophys. J.* **343** (1989) 169; S. Rudaz and F. Stecker, *Astrophys. J.* **368** (1991) 406; M. Urban *et al.*, *Phys. Lett. B* **293** (1992) 149; V. Berezhinsky, A. Gurevich and K. Zybin, *Phys. Lett. B* **294** (1992) 221; V. Berezhinsky, A. Bottino and G. Mignola, *Phys. Lett. B* **325** (1994) 136; L. Bergstrom, P. Ullio and J. H. Buckley, *Astropart. Phys.* **9** (1998) 137; L. Bergstrom, J. Edsjö and P. Ullio, *Phys. Rev. D* **58** (1998) 083507; J. Buckley *et al.*, [astro-ph/0201160](#); P. Ullio, L. Bergstrom, J. Edsjö and C. Lacey, *Phys. Rev. D* **66** (2002) 123502.
- [60] H. A. Mayer-Hasselwander *et al.* (EGRET Collaboration), MPE-440 (1998).
- [61] A. Morselli *et al.*, (GLAST Collaboration), *Nucl. Phys.* **113** (*Proc. Suppl.*) (2002) 213.
- [62] S. Rudaz and F. Stecker, *Astrophys. J.* **325** (1988) 16; A. Tylka, *Phys. Rev. Lett.* **63** (1989) 840; M. Turner and F. Wilczek, *Phys. Rev. D* **42** (1990) 1001; M. Kamionkowski and M. Turner, *Phys. Rev. D* **43** (1991) 1774; A. Moskalenko and A. Strong, *Phys. Rev. D* **60** (1999) 063003; E. Baltz and J. Edsjö, *Phys. Rev. D* **59** (1999) 023511; G. Kane, L. T. Wang and J. Wells, *Phys. Rev. D* **65** (2002) 057701; E. Baltz, J. Edsjo, K. Freese and P. Gondolo, *Phys. Rev. D* **65** (2002) 063511; G. Kane, L. T. Wang and T. Wang, *Phys. Lett. B* **536** (2002) 263; D. Hooper, J. Taylor and J. Silk, [hep-ph/0312076](#).
- [63] M. A. DuVernois *et al.* (HEAT Collaboration), *Astrophys. J.* **559** (2001) 296.
- [64] M. Pearce (Pamela Collaboration), *Nucl. Phys.* **113** (*Proc. Suppl.*) (2002) 314.
- [65] J. Casaus *et al.* (AMS Collaboration), *Nucl. Phys.* **114** (*Proc. Suppl.*) (2003) 259.
- [66] F. Stecker, S. Rudaz and T. Walsh, *Phys. Rev. Lett.* **55** (1985) 2622; F. Stecker and A. J. Tylka, *Astrophys. J.* **336** (1989) L51; P. Chardonnet, Mignola, P. Salati and R. Taillet, *Phys. Lett. B* **384** (1996) 161; A. Bottino, F. Donato, N. Fornengo and P. Salati, *Phys. Rev. D* **58** (1998) 123503; L. Bergstrom, J. Edsjo and P. Ullio, *Astrophys. J.* **526** (1999) 215.
- [67] S. Orito *et al.* (BESS Collaboration), *Phys. Rev. Lett.* **84** (2000) 1078.
- [68] H. Fuke *et al.* (BESS Collaboration), [astro-ph/0504361](#).
- [69] K. Mori, C. J. Hailey, E. A. Baltz, W. W. Craig, M. Kamionkowski, W. T. Serber and P. Ullio, *Astrophys. J.* **566** (2002) 604, C. J. Hailey *et al.*, *JCAP* **0601** (2006) 007 [[arXiv:astro-ph/0509587](#)].
- [70] S. Profumo and C.E. Yaguna, *Phys. Rev. D* **70** (2004) 095004
- [71] H. Baer and S. Profumo, *JCAP* **0512** (2005) 008.
- [72] D. Dicus, S. Nandi and X. Tata, *Phys. Lett. B* **129** (1983) 451; A. Chamseddine, P. Nath and R. Arnowitt, *Phys. Lett. B* **129** (1983) 445; H. Baer and X. Tata, *Phys. Lett. B* **155** (1985) 278; H. Baer, K. Hagiwara and X. Tata, *Phys. Rev. Lett.* **57** (1986) 294 and *Phys. Rev. D* **35** (1987) 1598; R. Arnowitt and P. Nath, *Mod. Phys. Lett. A* **2** (1987) 331;

- R. Barbieri, F. Caravaglios, M. Frigeni and M. Mangano, *Nucl. Phys.* **B 367** (1991) 28; H. Baer and X. Tata, *Phys. Rev.* **D 47** (1993) 2739; J. Lopez, D. Nanopoulos, X. Wang and A. Zichichi, *Phys. Rev.* **D 48** (1993) 2062 and *Phys. Rev.* **D 52** (1995) 142; H. Baer, C. Kao and X. Tata, *Phys. Rev.* **D 48** (1993) 5175; S. Mrenna, G. Kane, G. Kribs and J. Wells, *Phys. Rev.* **D 53** (1996) 1168; H. Baer, C. H. Chen, F. Paige and X. Tata, *Phys. Rev.* **D 54** (1996) 5866; K. Matchev and D. Pierce, *Phys. Rev.* **D 60** (1999) 075004; H. Baer, M. Drees, F. Paige, P. Quintana and X. Tata, *Phys. Rev.* **D 61** (2000) 095007; V. Barger, C. Kao and T. Li, *Phys. Lett.* **B 433** (1998) 328; V. Barger and C. Kao, *Phys. Rev.* **D 60** (1999) 115015; K. Matchev and D. Pierce, *Phys. Lett.* **B 467** (1999) 225; H. Baer, T. Krupovnickas and X. Tata, *J. High Energy Phys.* **0307** (2003) 020.
- [73] H. Baer, J. Ellis, G. Gelmini, D. V. Nanopoulos and X. Tata, *Phys. Lett.* **B 161** (1985) 175; G. Gamberini, *Z. Physik* **C 30** (1986) 605; H. Baer, V. Barger, D. Karatas and X. Tata, *Phys. Rev.* **D 36** (1987) 96; H. Baer, X. Tata and J. Woodside, *Phys. Rev.* **D 45** (1992) 142.
- [74] H. Baer and E. Berger, *Phys. Rev.* **D 34** (1986) 1361; H. Baer, X. Tata and J. Woodside, *Phys. Rev. Lett.* **63** (1989) 352, *Phys. Rev.* **D 41** (1990) 906 and *Phys. Rev.* **D 44** (1991) 207; H. Baer, C. Kao and X. Tata, *Phys. Rev.* **D 48** (R2978) 1993; H. Baer, C. H. Chen, C. Kao and X. Tata, *Phys. Rev.* **D 52** (1995) 1565; H. Baer, C. H. Chen, F. Paige and X. Tata, *Phys. Rev.* **D 54** (1996) 5866; H. Baer, C. H. Chen, M. Drees, F. Paige and X. Tata, *Phys. Rev.* **D 58** (1998) 075008. For an overview, see S. Abel *et al.*, Report of the mSUGRA working group for the workshop on Physics at Run II at the Tevatron, [hep-ph/0003154](#).
- [75] See H. Baer, M. Drees, F. Paige, P. Quintana and X. Tata, Ref. [72].
- [76] H. Baer, C. H. Chen, F. Paige and X. Tata, *Phys. Rev.* **D 52** (1995) 2746 and *Phys. Rev.* **D 53** (1996) 6241; H. Baer, C. H. Chen, M. Drees, F. Paige and X. Tata, *Phys. Rev.* **D 59** (1999) 055014; S. Abdullin and F. Charles, *Nucl. Phys.* **B 547** (1999) 60; S. Abdullin *et al.* (CMS Collaboration), [hep-ph/9806366](#); B. Allanach, J. Hetherington, A. Parker and B. Webber, *J. High Energy Phys.* **08** (2000) 017.
- [77] H. Baer, K. Hagiwara and X. Tata, *Phys. Rev.* **D 35** (1987) 1598; H. Baer, D. Dzialo-Karatas and X. Tata, *Phys. Rev.* **D 42** (1990) 2259; H. Baer, C. Kao and X. Tata, *Phys. Rev.* **D 48** (1993) 5175; H. Baer, C. H. Chen, F. Paige and X. Tata, *Phys. Rev.* **D 50** (1994) 4508. I. Hinchliffe *et al.*, *Phys. Rev.* **D 55** (1997) 5520 and *Phys. Rev.* **D 60** (1999) 095002; H. Bachacou, I. Hinchliffe and F. Paige, *Phys. Rev.* **D 62** (2000) 015009; Atlas Collaboration, LHCC 99-14/15; C. Lester, M. Parker and M. White, *J. High Energy Phys.* **0601** (2006) 080.
- [78] H. Baer, V. Barger, G. Shaughnessy, H. Summy and L. T. Wang, *Phys. Rev.* **D 75** (2007) 095010.
- [79] H. Bachacou, I. Hinchliffe and F. Paige, Ref.[77]
- [80] R. Kitano and Y. Nomura, *Phys. Rev.* **D 73** (2006) 095004. More generally, the shape of the dilepton mass distribution may also depend on other parameters as discussed by M. Nojiri and Y. Yamada, *Phys. Rev.* **D 60** (1999) 015006; H. Baer, M. Drees, F. Paige, P. Quintana and X. Tata, Ref. [72]; M. Drees, Y. G. Kim, M. M. Nojiri, D. Toya and K. Hasuko, *Phys. Rev.* **D 63** (2001) 035008; A. Birkdal, R. C. Group and K. Matchev, [hep-ph/0507002](#); D. J. Miller, P. Osland, A. R. Raklev, *J. High Energy Phys.* **0603** (2006) 034.
- [81] H. Baer, A. Belyaev, T. Krupovnickas and X. Tata, *J. High Energy Phys.* **0402** (2004) 007; H. Baer, T. Krupovnickas and X. Tata, *J. High Energy Phys.* **0406** (2004) 061; see also H. Baer, R. Munroe and X. Tata, *Phys. Rev.* **D 54** (1996) 6735.

- [82] S. Y. Choi, A. Djouadi, M. Guchait, J. Kalinowski, H. S. Song and P. M. Zerwas, *Eur. Phys. J. C* **14** (2000) 535; S. Y. Choi, J. Kalinowski, G. A. Moortgat-Pick and P. M. Zerwas, *Eur. Phys. J. C* **22** (2001) 563, and Addendum *ibid* **C23** 2002 69.